Theoretical Prediction of Nuclear Magnetic Shielding Constants of Acetonitrile

Ahmad Y. Adam

Thesis submitted to the Faculty of the
Virginia Polytechnic Institute and State University
in partial fulfillment of the requirements for the degree of

Master of Science
in
Chemistry

Richard D. Gandour, Chair
Diego Troya
Edward F. Valeev

May 10, 2012
Blacksburg, Virginia

Keywords: Acetonitrile, Magnetic Properties, Quantum Chemical Models, Molecular Dynamics Simulation

Theoretical Prediction of Nuclear Magnetic Shielding Constants of Acetonitrile

Ahmad Y. Adam

(ABSTRACT)

Gauge invariant shielding constants calculations of ^{1}H, ^{13}C, and ^{15}N were calculated for acetonitrile in the gas and liquid phases. Different basis sets as well as different *ab initio* and DFT methods were tested to select a time-efficient level of theory with reasonable accuracy. The effect of nuclear motion on the shielding constants was also explored. To investigate solvent effects on the shielding constants of acetonitrile, different clusters were extracted from molecular dynamics simulations. Convergence to the experimental values varied for the different clusters. The geometry of the central molecule in a cluster played an important factor in reaching convergence.

Contents

List of Figures

List of Tables

Chapter 1

Introduction and Literature Review

1.1 The NMR Chemical Shift

One of the most powerful techniques used in chemistry for the elucidation of molecular structures is the nuclear magnetic resonance (NMR) [1]. The significance of this field of research cannot be ignored as illustrated by three Nobel Prizes in Physics, Chemistry and Medicine in 1952, 1992 and 2003, respectively [2]. The output from an NMR experiment is the so-called the chemical shift spectrum. The basic two pieces of information that chemists extract from NMR spectra are the chemical shifts and the spin-spin coupling constants. The chemical shift is defined as the fractional variation of the resonance frequency of the nuclear spin due to its magnetic environment [3]. The response of the nuclear spins to the change in their environment can be used to elucidate molecular structure. The connection between an NMR spectrum and molecular structure is not always trivial. For example, in the case of vannusal B a new assigned structure was proposed [4]. This was done with the aid of computational methods. The application of computational methods to calculate the chemical shifts of ^{1}H and ^{13}C in complex organic molecules was recently reviewed [5].

Nowadays, in the field of chemical research, theory has matured to a state that allows a partnership with experiment. Theory and computation in chemistry help us to confirm, interpret, and predict experimental results. This can be seen from a recent Nobel Prize in chemistry in 1998, which was awarded for the development of *ab initio* and density-functional methods in computational chemistry. Many molecular properties can now be calculated with high accuracy [6] [7].

Modeling of NMR spectra of molecules is not straightforward. The chemical shift of a nucleus is computed as the difference between the nuclear magnetic shielding constants of the corresponding nuclei in the sample molecule and a reference compound. Electronic structure theory [8] can be used to compute shielding constants. Application of electronic structure theory approach to computation of NMR shielding constants involves many factors: the choice of molecular geometry, the size of the basis set to model the electronic distribution, and the number of electronic configurations included to account properly for the correlated motion of electrons. Other factors must also be considered, such as how many stable conformers a molecule can access, the rovibrational motion of molecules at room temperature, and electric field perturbation on the molecular system under study, which is represented by solvents in the case of liquid-phase experiments [9], here to be taken into consideration.

In addition to the presence of the sample and reference compounds in the system under study, there is also the solvent. Most solvents have active NMR nuclei and that is why their presence are in very few amounts and in deuterated forms. Acetonitrile is among the common solvents used in NMR experiments. In this study, we discuss quantum chemical models [10] to compute the nuclear magnetic shielding constants of acetonitrile with wave function and density functional electronic structure methods, with and without incorporation of the nuclear dynamical effects. Before discussing our results, a brief introduction to predicting shielding constants (hence, chemical shifts) is in order.

1.2 Computation of the Chemical Shift

1.2.1 Empirical Methods

A quick and automated way to calculate chemical shifts is empirical methods (also known as incremental methods). The input is only the molecular structure, then based on a large set of data of chemical shifts of different nuclei in various environments the chemical shift of the input structure is calculated in few seconds [11]. Examples of empirical programs are ChemDraw and ACD [12]. A more developed approach is based on neural network in which the code is able to predict the molecular structure with the spectrum only as the input [13]. However, the application of these methods is not always successful because this depends on how many similar structures are available in the libraries of the software packages. Unusual molecular structures and stereochemistry [14] are the main challenges for empirical methods and lay outside their current abilities.

An alternative route and a more sophisticated one, but computationally more expensive, is quantum mechanical methods. Although the laws of quantum mechanics were completed in 1926, the application of these laws to chemical problems, and specially NMR calculations, was not immediate for reasons described in the following sections.

1.2.2 Classic Work and the Gauge Problem

Ramsey formulated the theory of nuclear magnetic shielding a long time ago [15]. In the 1960s, Hameka emphasized that different gauge origins gave different magnetic properties [16]. Because of the gauge-origin problem, substantial progress in computing the NMR spectra did not start until the 1990s. Cybulski and Bishop [17] avoided the gauge-origin dependency by using large basis set where they applied third-order Møller-Plesset (MP3)

theory and linearized coupled-cluster double excitation (L-CCD) theory on small molecules. Chesnut et al. [18] proposed using locally dense basis sets in the calculation of the nuclear magnetic shielding constant. In this approach, large basis sets were used for the molecular fragments that include the nuclei of interest while smaller basis sets are used for the rest of the molecule.

Using very large basis sets in order to avoid the gauge-origin problem will block the application of high-accurate quantum chemical methods to large molecules because of the high degree of computational scaling of such methods with the system size. To overcome this challenge, researchers developed several methods: individual gauges for atoms in molecules (IGAIM) [19], the individual gauge for localized orbitals (IGLO) [20], Localized Orbitals/Localized Origins (LORG) [21], and gauge-invariant atomic orbitals (GIAO). Our choice for the proposed project in the following chapters was the GIAO method.

In 1937, Fritz London developed GIAO [22], which were used by Hameka in 1965 [16] in the calculation of magnetic shielding constants of diatomic molecules, and later by Ditchfield [23] to derive the HF perturbation theory for magnetic properties with an application by Fukui et al. on H_2O [24]. In 1990, Wolinski et al. demonstrated that GIAO is an efficient method in terms of basis set convergence [25]. Helgaker and Jørgensen [26] subsequently formulated the GIAO approach for ab initio methods.

1.2.3 Geometry Dependence

Choosing the GIAO approach, the next question was: Which level of theory to use for geometry optimization before computing magnetic shielding constants. Jaszunski et al. [27] reported that different values reported in the literature for ^{13}C chemical shifts in tetrachlorocyclopropene were due to different molecular geometries. Zhang et al. [28] tested three dif-

ferent optimized geometries for a set of 18 small molecules with a range of 1 - 6 heavy atoms. The optimization was at HF, BLYP, and B3LYP levels of theory, all with the 6-31G(d) basis set, and the ^{13}C magnetic shielding constant calculations were at the B3LYP/6-311+G(2d,p) level. The best approach was B3LYP/6-311+G(2d,p)//HF/6-31G(d) with a mean absolute deviation of 2.36 ppm with respect to experiment. The HF optimized geometry helped to balance the deshielding tendency of the B3LYP method. The B3LYP//HF approach was successful with a larger molecule (versicolorin C_{18} H_{13} O_7) in comparison to the experimental values of ^{13}C chemical shifts.

At the post-Hartree-Fock level, Auer et al. [29] considered MP2/cc-pVTZ, CCSD(T)/cc-pVTZ, and CCSD(T)/cc-pVQZ levels of theory for geometry optimization for a set of 16 small polyatomic molecules for the calculations of ^{13}C chemical shifts. They selected CCSD(T)/cc-pVTZ geometries, which did not differ significantly from the more accurate CCSD(T)/cc-pVQZ geometries and were better than MP2/cc-pVTZ geometries. However, they indicated there was no great geometry dependence, except with CO, because all levels of theory are considered accurate for obtaining equilibrium geometries.

1.2.4 Basis Sets

Basis sets are mathematical functions that describe the motion of electrons and they are required as an input for the calculations of chemical shifts. In the literature, there are several categories of basis sets, with different type and number of functions, designed to approach the basis set limit [30]. As discussed above, using very large basis sets solves the gauge-origin problem.

Usually larger basis sets provide more accurate results than those with smaller ones but this was not the case with Jain et al. [31]. They found a larger error in B3LYP calculations of

^{1}H chemical shift with cc-pVTZ than the error with cc-pVDZ. At the HF level, with smaller basis sets may gave a better results [32], but this can be attributed to cancellation of errors. These errors introduced by using truncated basis sets and the error by treating the correlated motion of the electrons improperly in HF theory [33].

Smith et al. [34] used different basis sets at the HF-SCF level of theory and concluded that the LORG method provided reliable results for ^{13}C chemical shifts magnetic shielding constants in a series of cyclopropene derivatives. On the same model molecules, Jaszunski et al. [35], however, found GIAO method performed better than IGLO and LORG approaches. Further, van Wulen et al. [36] suspected that results at the HF level of theory for cyclopropene derivatives [34] could be taken for granted at the HF level of theory without studying electron correlation effects. Cheeseman et al. [37] used two different families of basis sets, the so-called Pople basis sets and Ahlrichs basis sets. They emphasized the conclusion that basis sets converged faster with the GIAO method than with the CSGT method for both HF and DFT. They also found that the 6-31G* basis set gave comparable results for ^{13}C chemical shifts to those of the larger basis set 6-311+G(2d,p).

Auer et al. [29] investigated the basis-set error at the CCSD(T) level in basis sets developed by Schäfer et al. [38]. The convergence behavior of tested basis sets was compared to the performance of a large basis set, 13s9p4d3f . The QZ2P basis set (with its 1-5 ppm deviation from the complete basis-set limit) demonstrated a good choice for testing correlation effects.

For computing shielding constants, Jesnen [39] [40] designed basis sets that included tight functions in its structure. These basis sets gave lower error than others available and were used in the current study.

1.2.5 Electron Correlation

Accurate calculations of shielding constants require a precise description of the electronic structure of molecules. The HF method is not sufficient to treat the correlated motion of electrons properly. It is a one-electron theory in which an electron feels an average field from all other electrons. After Wolinski et al.'s [25] seminal work on the efficiency of the GIAO method, different research groups started during 1990s implementing the GIAO method for different electron correlation approaches. The work started with one of the simplest ab initio methods to treat electron correlation, MP2, where Gauss [41], using the GIAO method (GIAO-MBPT(2)), studied correlation effects on ^{17}O chemical shifts. The study was later extended to include ^{13}C and ^{15}N chemical shifts [42]. Using a higher order method like the third-order MP3 in the calculation of shielding tensors resulted in negative corrections compared to the MP2 method [43]. The study by Olsen et al. [44] proved that, in general, results from higher-order perturbation theory beyond MP2 are not guaranteed to converge. Multi-references based methods for treating electron correlation like the complete active space self-consistent field method (CASSCF) have also been used to compute nuclear magnetic shieldings [45]. However, CASSCF methods are not black-box methods and the selection of the active space requires understanding of the chemical problem [46].

Although MP2 is an electron correlated method, but there are some molecular cases [47] that require more accurate methods like coupled-cluster methods. Coupled-cluster theory emerged during the late 1980s and became the most successful wave-function based method in treating dynamical electron correlations [48]. Gauss and Stanton developed several versions of coupled-cluster methods to calculate nuclear shielding constants [49] [50] [51] [52] [53]. These were later benchmarked for different nuclei [29] [54] [55]. In a study on ^{13}C shielding constants [29], they used HF-SCF, MP2, CCSD, CCSD(T) levels of theory to test correlation effects on a series of small closed-shell molecules with size ranging from 1 - 5 heavy

atoms. The HF-SCF method produced an error of 35 ppm relative to CCSD(T) method for shielding constants. However, HF-SCF method performed better for chemical shifts due to cancellation of errors (as the error in computing ^{13}C shielding constants will be systematic among molecules under study and reference compounds).

1.2.6 DFT

The advantage in the speed of computations by DFT over wave-function methods attracted researchers to utilize DFT in calculations of nuclear shielding constants [56] [57] [58] [59] [60] [61]. However, the semi-empirical implementation of DFT methods does not allow an ultimate functional [62] to be used for any molecular property that interests us. The performance of DFT methods requires comparison to experiment, HF method, and post HF methods to test how much correlation effects have been recovered by DFT. Cheesman et al. [37] tested the performance of different DFT functionals versus HF method, MP2 method, and experiment. They found that DFT methods were useful in comparison to the HF-SCF method. In comparison to coupled-cluster methods [29], DFT-BP86 and DFT-B3LYP methods underestimated the ^{13}C shielding constant in a set of 16 molecules with size ranging from 1 - 5 heavy atoms (up to -30 ppm). However, these are systematic errors, which will probably be cancelled in chemical shifts computation. In a recent study by Jain et al. [63], they were looking for the best accuracy/cost ratio of different functionals in a set of 80 conformationally stable molecules; WP04 and B3LYP with the basis set 6-31G** provided reliable results for chemical shifts.

B3LYP is one of the widely used functional among DFT methods and has been used in shielding constant calculations [37] [29] . In 2009, Kupka demonstrated that BhandH functional performed better in shielding constant calculations compared to B3LYP [64] [65].

BHandH functional was our choice to calculate the shielding constants of liquid acetonitrile (represented by different clusters extracted from molecular dynamics simulations).

1.2.7 Rovibrational Effects

Molecules are never at rest; even at 0 K, they vibrate. At higher temperatures there is a coupled rovibrational motion. To achieve accuracy in the calculated shielding constants, the rovibrational effects need to be taken into account [66]. Sundholm et al. using the GIAO technique with coupled-cluster theory [67] obtained the rovibrational corrections to shielding constants for a series of diatomic molecules (H_2, HF, N_2, CO, and F_2); when comparison were made to experimental values, these corrections reduced the error in computed results. In another example, adding rovibrational estimates to the shielding constant of the oxygen nucleus in the water molecule produced a new shielding scale. This shielding scale improved the theoretical value of the oxygen chemical shift in carbon monoxide. For small polyatomic molecules within the range of 1 - 5 heavy atoms, vibrational effects resulted in systematic corrections (-0.5 to -4.5 ppm). While these corrections are important for absolute shielding, their effects will be minimized in case of chemical shifts [29].

1.2.8 Solvent Effects

Usually NMR experiments are done in the liquid phase; therefore, the effect of solvents on shielding constants cannot be ignored. The accuracy of *ab initio* [42] and DFT methods [37] to compute shielding constant in the gas phase is not transferrable to molecules in solutions and a further step is needed to account for solvent effects [68] [69]. The effect of solvation on NMR chemical shifts was first observed in 1957 [70] [71]. Theoretical analysis of solvent effects on nuclear shielding constants dated back to the work of Buckingham et

al. [72]. The solvent effects were categorized as four components that add to value of the isolated shielding constant in the gas phase. The components are due to van der Waals interactions, solvent magnetic anisotropy, polar effects, and bulk magnetic susceptibility. In the study, specific solvent effects like hydrogen bonding were not considered explicitly. Nowdays, modern research approaches, computationally, the solvation phenomena with two main strategies, implicit and explicit modeling of the solvent [9].

Implicit Models

The Polarizable Continuum Model (PCM) treats the solvent as a continuum dielectric medium and solute molecules are placed in a cavity of defined size and shape [73]. Mikkelsen et al. [74] used the PCM model with the multi-configurational self-consistent reaction-field method (MCSCRF) on water and methane molecules in a range of solvents with different dielectric constants (ϵ) (from pentane (ϵ=1.84) to water (ϵ=78.54)) . The value of the shielding constant increased for ^{17}O and ^{13}C nuclei, while it decreased for hydrogens nuclei with increasing the dielectric constant of the medium. It should be noted that, the PCM model is insufficient to treat the shielding constant of the ^{17}O nucleus in liquid water because there are no hydrogen bonds accounted for in the model [75]. In a study on ^{1}H, ^{13}C, ^{15}N, and ^{17}O nuclei, Benzi et al. [76] recommended treating explicitly the first shell of solvent molecules, when dealing with hydrogen-bonded systems.

In a study on the shielding constants of water and methane the authors found that electronegative atoms were shielded with increasing the dielectric constant in the continuum model and the others atoms were deshielded [74].

Explicit Models

A more realistic approach compared to the continuum implicit model is to treat the solvent explicitly with molecular structures. The positions and geometries of the solvent molecules could be determined via molecular dynamics simulations. Then from the output of the simulation a cluster with specific size is extracted and used as an input for quantum chemical calculations of the molecular property of interest. Small molecules like H_2O, H_2S, and HCN were candidates for calculating shielding constants by quantum mechanics/molecular dynamics [75] [77]. The NMR spectrum of ethanol in the liquid phase was studied with MD/QM technique [78]. The MD box contained 100 ethanol molecules (d= 0.787 g/cm^3) and simulation was run with OPLS/AA force field for 250 ps. Radial distribution function (RDF) was used to define the cluster size for QM calculations. Due to the existence of hydrogen bonds in liquid ethanol, the authors also carried hydrogen bond analysis. Different clusters were analyzed with the size varied from 3 – 13. However, the authors chose to trace on one ethanol molecule, and its environment, at different time frames. In their approach, they were able to predict the experimental value of the hydroxyl proton within a reasonable value in contrast to a previous work [79].

1.3 Acetonitrile

Acetonitrile is a polar aprotic solvent, with large dipole moment (3.9 D) [80], used in organic and electrochemistry. In the liquid phase, the intermolecular force is dipole-dipole interaction [81] with anti-parallel configuration [82] as preference. This pair stability of acetonitrile molecules led to the conclusion that clusters of even number of molecules are more stable than those with odd numbers [83] [84]. Theoretically, the structure of liquid acetonitrile has also been investigated. In 1983, Bohm et al. developed an intermolecular potential

for acetonitrile for molecular dynamics simulations that provided a good agreement with experimental thermodynamic data [85]. Also Monte Carlo simulations have been used to study liquid acetonitrile [86]. The important role of dipole-dipole interaction in the structure of acetonitrile has also been shown computationally [87]. Calculations by Siebers et al. showed the anti-parallel dimer as a building entity of acetonitrile clusters [88]. Ab initio and DFT methods were also used to investigate the structure of acetonitrile [89] [90].

The question of how the structure of acetonitrile in the liquid phase will change the gas phase NMR data is investigated in this thesis. The study of gas-liquid changes of spectroscopic parameters is a tool to understand the phenomena of solvent effects. We used molecular dynamics to simulate acetonitrile in the liquid phase and chose 9 clusters. We explored the number of molecules in a cluster needed for convergence. We have explored the magnetic shielding constants of ^{1}H, ^{13}C, and ^{15}N by examining the basis set limits for HF, MP2, CCSD, and DFT methods in the gas phase.

Chapter 2

Computational Details For Gas Phase Calculations

Gaussian programs [91] were used for HF-SCF, second-order Møller–Plesset perturbation theory (MP2), and DFT calculations, while CFOUR program [92] was used for coupled-cluster calculations. Electronic structure methods used to compute ^{1}H, ^{13}C, and ^{15}N nuclear magnetic shielding constants of acetonitrile were HF-SCF, MP2, coupled-cluster singles and doubles (CCSD), BHandH, and B3LYP. No frozen-core approximation was used in the calculations. Gauge including atomic orbitals (GIAOs) have been used to avoid gauge-origin problems [25]. The input geometries for acetonitrile ranges from equilibrium structures (r_e) provided by high level calculations (MP2/cc-pVTZ, this work) to substitution (r_s) and effective (r_0) structures [93]. Basis-set series, Table 2.1, developed by Dunning [94] [95] [96], Ahlrichs [97] [98], Jensen [39] [40], and Gauss [42] were used in the study. In order to compare the computed shielding constants to the experimental data [99] vibrational effects were also computed at the HF-SCF level [100] [101]. Calculations were carried out on Intel Xeon (quad-core) 64-bit processor machines, CentOS (5.3) operating system.

Table 2.1: **Description of the various basis sets used in acetonitrile shielding constants calculations. Number of functions for each atom and the total number of functions for acetonitrile are given.**

Basis	H	C, N	Functions
- Dunning -			
cc-pVDZ	2s1p	3s2p1d	57
cc-pCVDZ	2s1p	4s3p1d	69
aug-cc-pVDZ	3s2p	4s3p2d	96
aug-cc-pCVDZ	3s2p	5s4p2d	108
cc-pVTZ	3s2p1d	4s3p2d1f	132
cc-pCVTZ	3s2p1d	6s5p3d1f	171
aug-cc-pVTZ	4s3p2d	5s4p3d2f	207
aug-cc-pCVTZ	4s3p2d	7s6p4d2f	246
cc-pVQZ	4s3p2d1f	5s4p3d2f1g	255
cc-pCVQZ	4s3p2d1f	8s7p5d3f1g	342
- Ahlrichs -			
SV(P)	2s	3s2p1d	48
SVP	2s1p	3s2p1d	57
TZVP	3s1p	5s3p2d1f	111
TZVPP	3s2p1d	5s3p2d1f	135
QZVP	4s3p2d1f	7s4p3d2f1g	261
- Jensen -			
pcS-0	2s	3s2p	33
pcS-1	2s1p	3s3p1d	66
pcS-2	3s2p1d	4s4p2d1f	141
pcS-3	5s4p2d1f	6s8p4d2f1g	321
pcS-4	7s6p3d2f1g	8s10p6d3f2g1h	543
ccJ-pVDZ	4s2p	6s3p2d	105
ccJ-pVTZ	5s3p2d	7s4p3d1f	195
ccJ-pVQZ	6s4p3d1f	9s5p4d2f1g	321
- Gauss -			
svp	2s1p	3s2p1d	57
dzp	2s1p	4s2p1d	60
tzp	3s1p	5s3p1d	75
tz2p	3s2p	5s3p2d	99
qz2p	4s2p	6s4p2d	114
pz3d2f	5s3p2d	8s5p3d2f	228
13s9p4d3f	8s3p2d	13s9p4d3f	324

Chapter 3

The Selection of Basis Sets

In order to find the most efficient combination of method and basis set for computing the shielding constants for acetonitrile, we first established what is the smallest basis set that would give a reasonably accurate result for shielding constants of the four nuclei (^{1}H, $^{13}CH_3$, ^{13}CN, and ^{15}N) shielding constants. Our approach required defining the basis set convergence limits for each nuclei. The highly accurate CCSD method with the optimized geometry at the MP2/cc-pVTZ level [102] was used with several series of basis sets (Table 2.1). The calculations gave simultaneously the convergence limits all four shielding constants (σ's), which are discussed individually in the following four sections.

3.1 ^{1}H Shielding Constant

The basis set convergence limit was defined by plotting the calculated σ's from all the basis sets as a function of the total number of the basis functions for acetonitrile (Figure 3.1). Approximately 200 basis functions were required to reach convergence–$\sigma(^{1}H)\sim$ 30.0 ppm. Previous studies [103] used HF and B3PW91 with aug-cc-VxZ (x=D–5, 96–621 functions) to

obtain the exponentially fitted convergence limits 30.2 and 29.6 ppm, respectively. We used six different series of basis sets. The different series of basis sets showed varied behavior in reaching convergence. The convergence limit depended on the total number of basis functions more than the type of basis functions in each series.

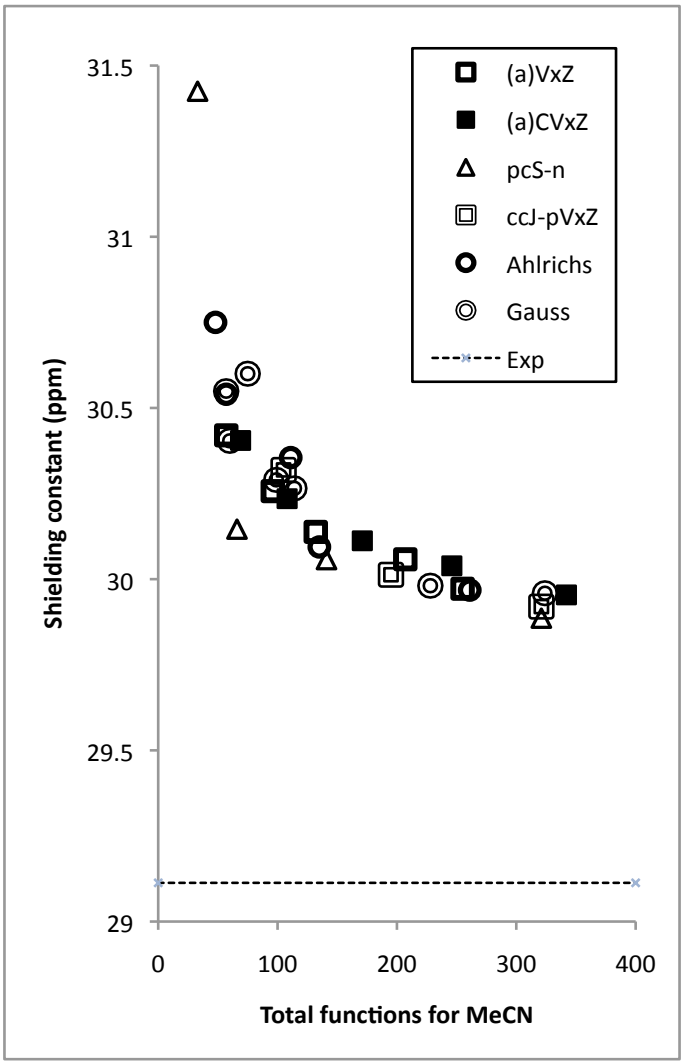

Figure 3.1: ^{1}H shielding constant of acetonitrile calculated by (CCSD//MP2/cc-pVTZ) versus the total number of functions with different basis sets.

The total change in $\sigma(^1\text{H})$ computed by Dunning's basis sets is 0.4 ppm (Table 3.1). The change occurs in the following increments: 0.2 ppm from cc-pVDZ (57 functions) to aug-cc-pCVDZ (108 functions), 0.1 ppm from aug-cc-pCVDZ to cc-pVTZ (132 functions), and

0.1 ppm from cc-pVTZ to aug-cc-pCVTZ (246 functions). The approach to convergence depended on the total number of basis functions rather than on the type of functions. For example, adding more core functions to treat core and core-valence correlation effects [96] has no effect as would be expected for ^{1}H. Augmented basis sets showed improvements inasmuch as the number of functions are increased. As the quality of basis sets increased from DZ to QZ, $\sigma(^1\text{H})$ decreased.

The total change in $\sigma(^1\text{H})$ computed by Ahlrichs's basis sets was 0.8 ppm (Table 3.1). In terms of number of functions, basis sets ranged from SV(P) (48 functions) to QZVP (261 functions); convergence occurs (30.0 ppm) with 261 functions. The addition of p-type functions, SVP basis set, resulted in deshielding by 0.3 ppm. Using TZVP, further deshield by 0.1 ppm occurred in contrast to the 0.3 ppm change upon moving from cc-pVDZ to cc-pVTZ in Dunning's basis sets. The reason may be due to the extra p- and d-type functions in cc-pVTZ compared to TZVP. Ahlrichs's and Dunning's TZ basis sets–TZVPP (135 functions) and to cc-pVTZ (132 functions)–produced 30.1 ppm for $\sigma(^1\text{H})$. In order to obtain the convergence limit (30.0 ppm), QZVP (261 functions) which is similar to cc-pVQZ (255 functions) was needed.

The total change in $\sigma(^1\text{H})$ computed by Gauss's basis sets was 0.5 ppm (Table 3.1). In terms of number of functions, basis sets ranged from svp (57 functions) to $13s9p4d3f$ (324 functions); convergence occurred (30.0 ppm) with pz3d2f (228 functions). Convergence depended on the total number and type of basis functions. For example, tzp (75 functions) gave a 0.5 ppm higher value for $\sigma(^1\text{H})$ than that given by cc-pVTZ (132 functions) and TZVPP (135 functions) because they contain extra p-type plus d-type functions. This difference is minimized to 0.2 ppm with tz2p (99 functions), which has additional p-type functions compared to tzp. Increasing to qz2p (114 functions) gave the same value as tz2p. When d-type functions are added to ^{1}H (pz3d2f), the converged value is reached.

The total change in $\sigma(^1\text{H})$ computed by Jensen's pcS-n basis sets is 1.5 ppm (Table 3.1). In terms of number of functions, basis sets ranged from pcS-0 (33 functions) to pcS-3 (321 functions); convergence occurred (29.9 ppm) with pcS-3. The approach to convergence depends on the total number of basis functions and the type of functions. Adding *p*-type functions to ^{1}H (pcS-1, 66 functions) gave 30.1 ppm for $\sigma(^1\text{H})$. The other similar basis sets to pcS-1 (cc-pVDZ, SVP, svp, and dzp) predicted higher values for $\sigma(^1\text{H})$ by 0.3–0.4 ppm than that by pcS-1. Jensen showed that improved basis set convergence occurred "by addition of a single tight *p*-type basis function" [39]. Adding more *p*- and *d*-type functions, pcS-2 basis set, produced no further change for $\sigma(^1\text{H})$. Further deshielding in $\sigma(^1\text{H})$ came with pcS-3 basis set with the additional *f*- and extra *s*-, *p*-, and *d*-type functions. The result is the lowest value, 29.9 ppm, produced for $\sigma(^1\text{H})$ in contrast to the other basis sets employed in the study.

The other Jensen's basis sets, ccJ-pVxZ (x=D–Q) [40], designed specifically for spin-spin coupling constant calculations were tested also. The total change in $\sigma(^1\text{H})$ computed by ccJ-pVxZ basis sets is 0.4 ppm (Table 3.1). In terms of number of functions, basis sets ranged from ccJ-pVDZ (105 functions) to ccJ-pVQZ (321 functions). The basis set ccJ-pVTZ predicted 30.0 ppm for $\sigma(^1\text{H})$ (the converged value by Dunning's and Ahlrichs's basis sets) with only 195 functions. Increasing the number of functions from 195 functions to 321 functions (ccJ-pVQZ) resulted in a deshiedling by only 0.1 ppm.

These studies lead to several conclusions about calculating $\sigma(^1\text{H})$ in acetonitrile. The addition of both *p*- and *d*-type functions on hydrogen improves the basis sets convergence. In terms of the cost/accuracy ratio for calculating $\sigma(^1\text{H})$, pcS-1 (66 functions) gives a value close to the converged limit. Although the pcS-1 has no *d*-type functions, a single tight *p*-type function improves the calculation of $\sigma(^1\text{H})$. Finally the remaining error from the experimental value 29.1 ppm [99] (Figure 3.1) could be attributed to the geometry and vibrational

effects [104].

3.2 ^{13}C Shielding Constants

3.2.1 $^{13}CH_3$ Shielding Constant

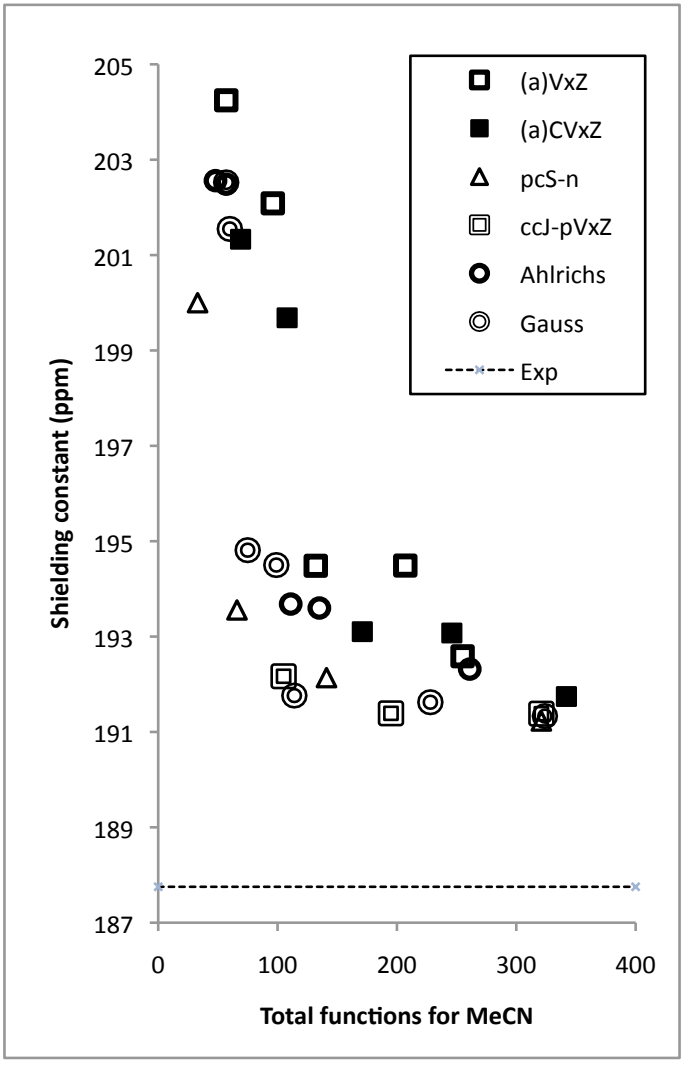

Figure 3.2: $^{13}CH_3$ shielding constant of acetonitrile calculated by (CCSD//MP2/cc-pVTZ) versus the total number of functions with different basis sets.

The convergence limit for $\sigma(^{13}CH_3)$ in acetonitrile, appears at $\sim$ 191.0 ppm (Figure 3.2).

Approximately 300 basis functions were required to reach convergence; however, some basis sets converged with fewer functions ($\sim$ 200). Previous studies [103] used HF and B3PW91 with aug-cc-VxZ (x=D–5, 96–621 functions) to obtain the exponentially fitted convergence limits 192.0 and 181.4 ppm, respectively. Another study [29] used CCSD and CCSD(T) with qz2p (114 functions) to obtain 192.3 and 192.1 ppm, respectively. We used six different series of basis sets, which showed varying behavior in reaching convergence. The convergence limit depended on the total number of basis functions and the type of basis functions in each series.

The total change in $\sigma(^{13}CH_3)$ computed by Dunning's basis sets is 12.5 ppm (Table 3.1). The change occurs in the following increments: 4.5 ppm from cc-pVDZ (57 functions) to aug-cc-pCVDZ (108 functions), 5.2 ppm from aug-cc-pCVDZ to cc-pVTZ (132 functions), 1.4 ppm from cc-pVTZ to aug-cc-pCVTZ (246 functions), 0.5 ppm from aug-cc-pCVTZ to cc-pVQZ (255 functions), and 0.9 ppm from cc-pVQZ to cc-pCVQZ (342 functions). The approach to the lowest value depended on the total number of basis functions and the type of functions. Adding more core functions [96] made deshielding changes (ppm): (2.4 and 2.9) DZ, (1.4) TZ, and (0.9) QZ. Augmented basis sets also showed deshielding changes (1.6 and 2.1 ppm) at the DZ level but not at the TZ level. As the basis sets changed from aug-cc-pVDZ to aug-cc-pVTZ, CCSD showed a large decrease, 202.1 to 194.5 ppm, in $\sigma(^{13}CH_3)$ similar to those calculated [103] with HF (201.6 to 194.4 ppm) and B3PW91 (193.2 to 185.9 ppm).

The total change in $\sigma(^{13}CH_3)$ computed by Ahlrichs's basis sets was 10.3 ppm (Table 3.1). In terms of number of functions, basis sets ranged from SV(P) (48 functions) to QZVP (261 functions); which gave the lowest value, 192.3 ppm. With TZVP, a deshielding of 8.8 ppm occurred similar to the 9.7 ppm change from cc-pVDZ to cc-pVTZ basis sets. Comparing respectively values of $\sigma(^{1}CH_{13})$, 193.6 and 194.5 ppm, calculated by TZVPP (135 functions)

and cc-pVTZ (132 functions) revealed an improvement with an additional s-type function on C and N atoms.

The total change in $\sigma(^{13}CH_{13})$ computed by Gauss's basis sets was 11.2 ppm (Table 3.1). In terms of number of functions, basis sets ranged from svp (57 functions) to $13s9p4d3f$ (324 functions); the lowest value occurred (191.3 ppm) with $13s9p4d3f$. The approach to the lowest value depended on the type of basis functions. The qz2p with only 114 functions gave a similar value (191.8 ppm) for $\sigma(^{1}CH_{13})$ to that (191.7 ppm) of cc-pCVQZ with 342 functions. With f-type functions in Gauss's basis sets (pz3d2f and 13s9p4d3f), the change in $\sigma(^{13}CH_3)$ is only 0.2–0.5 ppm. The changes in $\sigma(^{13}CH_3)$ as the number of functions increased compared favorably with the changes seen at the CCSD(T) level with CCSD(T)/cc-pVTZ geometry[29]: tzp (195.2 ppm), qz2p (192.1 ppm), pz3d2f (192.0 ppm), and 13s9p4d3f (191.7 ppm).

The total change in $\sigma(^{13}CH_3)$ computed by Jensen's pcS-n basis sets is 8.8 ppm (Table 3.1). In terms of number of functions, basis sets ranged from pcS-0 (33 functions) to pcS-3 (321 functions); the lowest value (191.2 ppm) occurred with pcS-3. The approach to the lowest value depended on the total number of basis functions and the type of functions. Adding d-type functions to (pcS-1, 66 functions) gave 193.6 ppm for $\sigma(^{13}CH_3)$. The other DZ similar basis sets to pcS-1 (cc-pVDZ, SVP, svp, and dzp) predicted higher values for $\sigma(^{13}CH_3)$ by $\sim$ 7.0 ppm than that by pcS-1. Jensen showed that improved basis set convergence occurred "by addition of a single tight p-type basis function" [39]. Adding more p- and d-type functions, pcS-2 basis set, produced small change (1.3 ppm) for $\sigma(^{13}CH_3)$. Further, 0.9 ppm deshielding in $\sigma(^{13}CH_{13})$ came with pcS-3 which has additional s-, p-, d-, and f-type, plus g-type functions. This resulted is in the lowest value for $\sigma(^{13}CH_3)$ in comparison to the other basis sets in this study.

The other Jensen's basis sets, ccJ-pVxZ (x=D–Q) [40], designed specifically for spin-spin

coupling constant calculations were tested also. The total change in $\sigma(^{13}CH_3)$ computed by ccJ-pVxZ basis sets is 0.8 ppm (Table 3.1). In terms of number of functions, basis sets ranged from ccJ-pVDZ (105 functions) to ccJ-pVQZ (321 functions). The basis set ccJ-pVTZ predicted 191.4 ppm for $\sigma(^{13}CH_3)$ (lower than the best values by Dunning's and Ahlrichs's basis sets) with only 195 functions. Increasing the number of functions to 321 functions (ccJ-pVQZ) resulted in no change in $\sigma(^{13}CH_3)$.

These studies lead to several conclusions about calculating $\sigma(^{13}CH_3)$ in acetonitrile. The addition of f-type functions on carbon does not improve the basis sets convergence; for example, tz2p and cc-pVTZ basis sets gave the same $\sigma(^{13}CH_3)$. Using basis sets at the TZ level have more influence on $\sigma(^{13}CH_3)$ more than the augmentation of the basis sets at the DZ level in Dunning's basis sets. Another factor that helps basis sets convergence is adding core functions. In terms of the cost/accuracy ratio for calculating $\sigma(^{13}CH_3)$, pcS-1 (66 functions; 193.6 ppm) gives a value close to the converged limit. One concludes that Jensen's basis sets converge to the limit with the fewest functions. A better basis set for $\sigma(^{13}CH_3)$ but with more functions is Gauss's qz2p (114 functions; 191.8 ppm). Finally the remaining error from the experimental value 187.8 ppm [99] (Figure 3.2) could be attributed to the geometrical and vibrational effects [29].

3.2.2 ^{13}CN Shielding Constant

The convergence limit ($\sim$ 72.0 ppm) for $\sigma(^{13}CN)$ in acetonitrile, appears below the experimental value 74.0 ppm (Figure 3.3). Approximately 200–350 basis functions were required to reach convergence; however, some basis sets converged with fewer functions ($\sim$ 140). Previous studies [103] used HF and B3PW91 with aug-cc-VxZ (x=D–5, 96–621 functions) to obtain the exponentially fitted convergence limits 69.3 and 59.7 ppm, respectively. Another

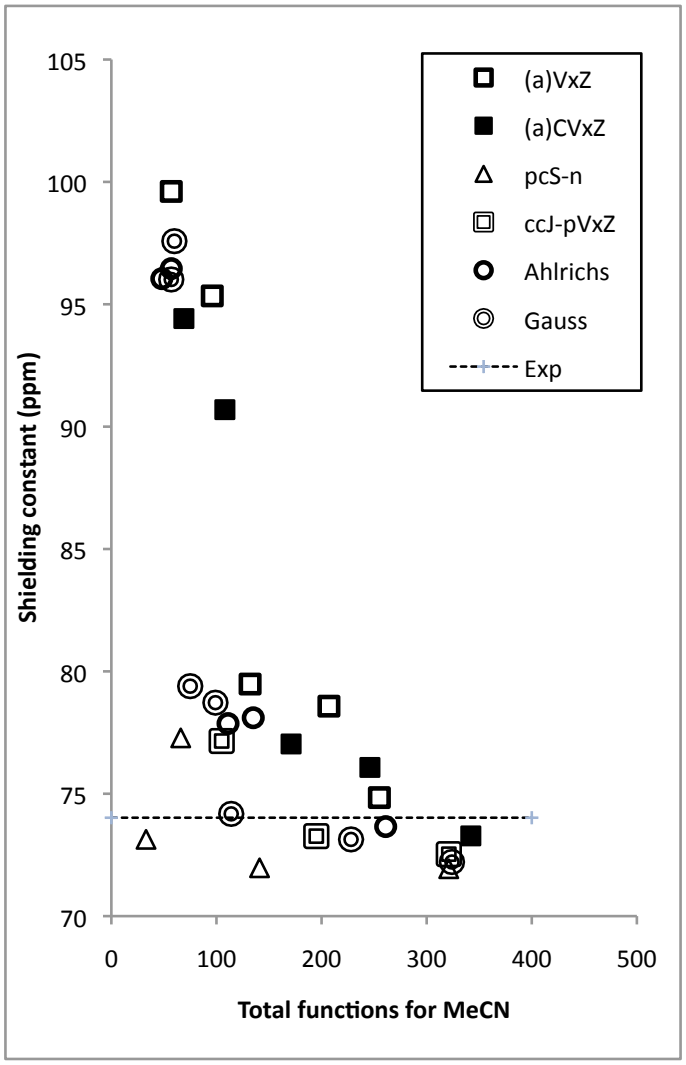

Figure 3.3: ^{13}CN shielding constant of acetonitrile calculated by (CCSD//MP2/cc-pVTZ) versus the total number of functions with different basis sets.

study [29] used CCSD and CCSD(T) with qz2p (114 functions) to obtain 76.2 and 78.2 ppm, respectively. We used six different series of basis sets, which showed varying behavior in reaching convergence. The convergence limit depended on the total number of basis functions and the type of basis functions in each series.

The total change in $\sigma(^{13}\text{CN})$ computed by Dunning's basis sets is 26.3 ppm (Table 3.1); the lowest value was 73.3 ppm. The change occurs in the following increments: 8.9 ppm from

cc-pVDZ (57 functions) to aug-cc-pCVDZ (108 functions), 11.2 ppm from aug-cc-pCVDZ to cc-pVTZ (132 functions), 3.4 ppm from cc-pVTZ to aug-cc-pCVTZ (246 functions), 1.3 ppm from aug-cc-pCVTZ to cc-pVQZ (255 functions), and 1.5 ppm from cc-pVQZ to cc-pCVQZ (342 functions) which gave the lowest value. Adding more core functions [96] made deshielding changes (ppm): (7.8 and 6.9) DZ, (2.5) TZ, and (1.5) QZ. Augmented basis sets also showed deshielding changes (4.3 and 3.7 ppm) at the DZ level and (0.9 ppm) at the TZ level. As the basis sets changed from aug-cc-pVDZ to aug-cc-pVTZ, CCSD showed a large decrease, 95.3 to 78.6 ppm, in $\sigma(^{13}\mathrm{CN})$ similar to those calculated [103] with HF (87.7 to 74.5 ppm) and B3PW91 (82.6 to 68.0 ppm).

The total change in $\sigma(^{13}\mathrm{CN})$ computed by Ahlrichs's basis sets was 22.3 ppm (Table 3.1). In terms of number of functions, basis sets ranged from SV(P) (48 functions) to QZVP (261 functions); which gave the lowest value, 73.7 ppm. With TZVP, a deshielding of 18.6 ppm occurred similar to the 20.1 ppm change from cc-pVDZ to cc-pVTZ basis sets. Comparing respectively values of $\sigma(^{13}\mathrm{CN})$, 78.1 and 79.5 ppm, calculated by TZVPP (135 functions) and cc-pVTZ (132 functions) revealed an improvement with an additional s-type function on C and N atoms.

The total change in $\sigma(^{13}\mathrm{CN})$ computed by Gauss's basis sets was 23.8 ppm (Table 3.1). In terms of number of functions, basis sets ranged from svp (57 functions) to $13s9p4d3f$ (324 functions); the lowest value (72.2 ppm) occurred with $13s9p4d3f$. The approach to the lowest value depended on the type of basis functions. The qz2p with only 114 functions gave a slightly higher value (74.2 ppm) for $\sigma(^{1}\mathrm{CN})$ to that (73.3 ppm) of cc-pCVQZ with 342 functions. With f-type functions in Gauss's basis sets (pz3d2f and 13s9p4d3f), the change in $\sigma(^{13}\mathrm{CN})$ is only 1.1–2.0 ppm. The decrease in $\sigma(^{13}\mathrm{CN})$ as the number of functions increased (Table 3.1) were consistently $\sim$ 4.0 ppm larger than those calculated at the CCSD(T) level with CCSD(T)/cc-pVTZ geometry[29]: tzp (83.5 ppm), qz2p (78.2 ppm), pz3d2f (77.3 ppm),

and 13s9p4d3f (76.4 ppm).

Calculations of $\sigma(^{13}\mathrm{CN})$ with Jensen's basis sets, pcS-n, showed an anomaly. The total change in $\sigma(^{13}\mathrm{CN})$ computed by Jensen's pcS-1 and pcS-3 basis sets is 5.3 ppm (Table 3.1). The value of $\sigma(^{13}\mathrm{CN})$ pcS-1 is shielded compared to pcS-0 value. In terms of number of functions, basis sets ranged from pcS-0 (33 functions) to pcS-3 (321 functions); the lowest value (72.0 ppm) occurred with pcS-2. The approach to the lowest value depended on the total number of basis functions and the type of functions. Adding d-type functions to $^{13}\mathrm{C}$ (pcS-1, 66 functions) gave 77.3 ppm for $\sigma(^{13}\mathrm{CN})$. The other DZ similar basis sets to pcS-1 (cc-pVDZ, SVP, svp, and dzp) predicted higher values for $\sigma(^{13}\mathrm{CN})$ by $\sim$ 20.0 ppm than that by pcS-1. Jensen showed that improved basis set convergence occurred "by addition of a single tight p-type basis function" [39]. Adding more p- and d-type functions, pcS-2 basis set, produced change (4.3 ppm) for $\sigma(^{13}\mathrm{CN})$. No further deshielding in $\sigma(^{13}\mathrm{CN})$ came with pcS-3 basis set with the additional s-, p-, d-, and f-type, plus g-type functions. The lowest value (72.0 ppm) produced for $\sigma(^{13}\mathrm{CN})$ in contrast to the other basis sets employed in the study.

The other Jensen's basis sets, ccJ-pVxZ (x=D–Q) [40], designed specifically for spin-spin coupling constant calculations were tested also. The total change in $\sigma(^{13}\mathrm{CN})$ computed by ccJ-pVxZ basis sets is 4.7 ppm (Table 3.1). In terms of number of functions, basis sets ranged from ccJ-pVDZ (105 functions) to ccJ-pVQZ (321 functions). The basis set ccJ-pVTZ predicted 73.3 ppm for $\sigma(^{13}\mathrm{CN})$ (similar to the best values by Dunning's and Ahlrichs's basis sets) with only 195 functions. Increasing the number of functions to 321 functions (ccJ-pVQZ) resulted in 0.8 ppm decrease in $\sigma(^{13}\mathrm{CN})$.

These studies lead to several conclusions about calculating $\sigma(^{13}\mathrm{CN})$ in acetonitrile. The addition of f-type functions on carbon does not improve the basis sets convergence; for example, tzp and cc-pVTZ basis sets gave similar $\sigma(^{13}\mathrm{CN})$).

Using basis sets at the TZ level have more influence on $\sigma(^{13}\mathrm{CN})$ more than the augmentation of the basis sets at the DZ level in Dunning's basis sets. Another factor that helps basis sets convergence is adding core functions. In terms of the cost/accuracy ratio for calculating $\sigma(^{13}\mathrm{CN})$, pcS-1 (66 functions; 77.3 ppm) gives a value close to the converged limit. It should be noted that the unpolarized basis set, pcS-0, gives a closer value. One concludes that Jensen's basis sets converge to the limit with the fewest functions. A better basis set for $\sigma(^{13}\mathrm{CN})$ but with more functions is Gauss's qz2p (114 functions; 74.2 ppm). Finally the remaining error from the experimental value 74.0 ppm [99] (Figure 3.2) could be attributed to the geometric effects [29].

3.3 ^{15}N Shielding Constant

The convergence limit $\sim$ –14.0 ppm for $\sigma(^{15}\mathrm{N})$ in acetonitrile (Figure 3.4), appears below the experimental value, –8.7 [99]. Approximately 300 basis functions were required to reach convergence; however, some basis sets converged with fewer functions ($\sim$ 140). Previous studies [103] used HF and B3PW91 with aug-cc-VxZ (x=D–5, 96–621 functions) to obtain the exponentially fitted convergence limits –26.5 and –37.7 ppm, respectively. Another study [105] with CCSD(T)/cc-pVQZ geometry used CCSD(T)/pz3d2f (228 functions) to obtain –3.5 ppm . We used six different series of basis sets, which showed varying behavior in reaching convergence. The convergence limit depended on the total number of basis functions and the type of basis functions in each series.

The total change in $\sigma(^{15}\mathrm{N})$ computed by Dunning's basis sets is 35.6 ppm (Table 3.1). The change occurs in the following increments: 3.5 ppm from cc-pVDZ (57 functions) to aug-cc-pCVDZ (108 functions), 26.2 ppm from aug-cc-pCVDZ to cc-pVTZ (132 functions), 0.3 ppm from cc-pVTZ to aug-cc-pCVTZ (246 functions), 3.3 ppm from aug-cc-pCVTZ to cc-pVQZ

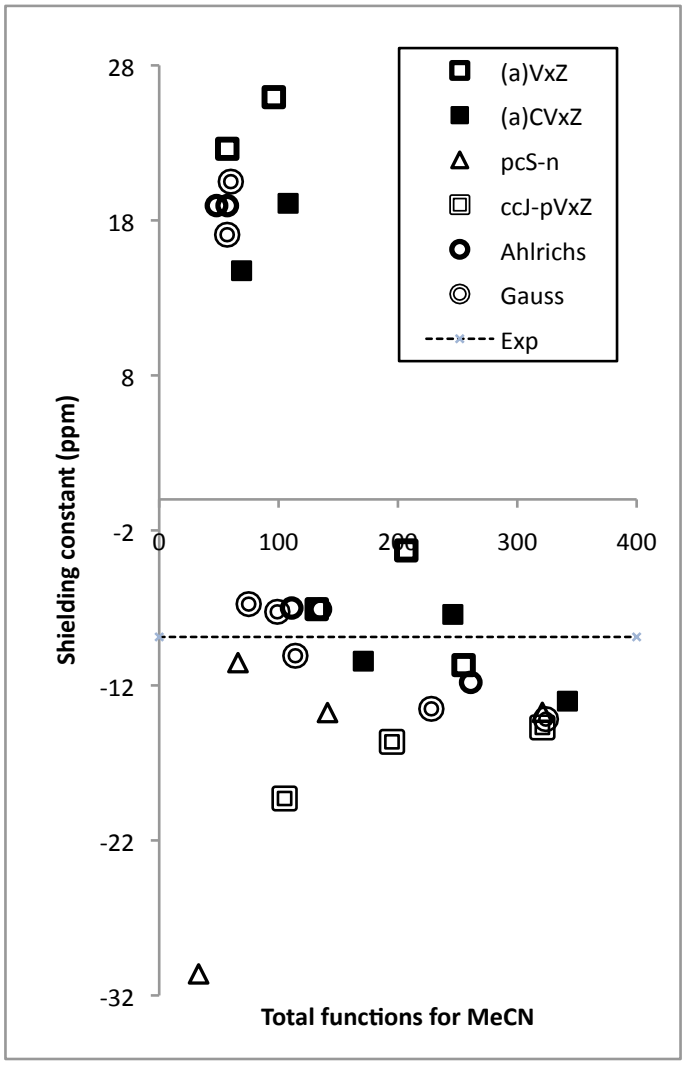

Figure 3.4: ^{15}N shielding constant of acetonitrile calculated by (CCSD//MP2/cc-pVTZ) versus the total number of functions with different basis sets.

(255 functions), and 2.3 ppm from cc-pVQZ to cc-pCVQZ (342 functions). The approach to convergence depended on the total number of basis functions and the type of functions. Adding more core functions [96] always made deshielding changes (ppm): (7.8 and 6.9) DZ, (3.3 and 4.1) TZ, (2.3) QZ. Unlike the case with $\sigma(^1\text{H})$ and $\sigma(^{13}\text{C})$, augmented basis sets showed shielding changes by (3.4 and 4.3 ppm) for DZ and (3.8 and 3.0 ppm) for TZ basis sets. As the basis sets changed from aug-cc-pVDZ to aug-cc-pVTZ, CCSD showed a large decrease, 26.0 to –3.3 ppm, in $\sigma(^{15}\text{N})$ similar to those calculated [103] with HF (3.5 to –17.7

ppm) and B3PW91 (0.7 to –23.9 ppm).

The total change in $\sigma(^{15}\mathrm{N})$ computed by Ahlrichs's basis sets was 30.8 ppm (Table 3.1). In terms of number of functions, basis sets ranged from SV(P) (48 functions) to QZVP (261 functions); which gave the lowest value, –11.8 ppm. With TZVP, a deshielding of 26.0 ppm occurred similar to the 29.7 ppm change from cc-pVDZ to cc-pVTZ basis sets. Comparing respectively values of $\sigma(^{15}\mathrm{N})$, –7.0 and –7.1 ppm, calculated by TZVPP (135 functions) and cc-pVTZ (132 functions) revealed no improvement with an additional s-type function on C and N atoms.

The total change in $\sigma(^{15}\mathrm{N})$ computed by Gauss's basis sets was 31.3 ppm (Table 3.1). In terms of number of functions, basis sets ranged from svp (57 functions) to $13s9p4d3f$ (324 functions); the lowest value (–13.5 ppm) occurred with $13s9p4d3f$. The approach to the lowest value depended on the type of basis functions. The qz2p with only 114 functions gave a higher value (-10.1 ppm) for $\sigma(^{15}\mathrm{N})$ to that (-13.0 ppm) of cc-pCVQZ with 342 functions. With f-type functions in Gauss's basis sets (pz3d2f and 13s9p4d3f), the change in $\sigma(^{15}\mathrm{N})$ is only 3.4–4.1 ppm.

The total change in $\sigma(^{15}\mathrm{N})$ computed by Jensen's pcS-0 and pcS-3 basis sets is $\sim$ 20.0 ppm (Table 3.1). In terms of number of functions, basis sets ranged from pcS-0 (33 functions) to pcS-3 (321 functions); lowest value (–31.0 ppm) occurred with pcS-0. The approach to convergence depends on the total number of basis functions and the type of functions. Adding d-type functions to $^{15}\mathrm{N}$ (pcS-1, 66 functions) gave –10.5 ppm for $\sigma(^{15}\mathrm{N})$. The other DZ similar basis sets to pcS-1 (cc-pVDZ, SVP, svp, and dzp) predicted positive values for $\sigma(^{15}\mathrm{N})$. Jensen showed that improved basis set convergence occurred "by addition of a single tight p-type basis function" [39]. Adding more p- and d-type functions, pcS-2 basis set, produced deshielding change (3.2 ppm) for $\sigma(^{15}\mathrm{N})$. No noticeable deshielding in $\sigma(^{15}\mathrm{N})$ came with pcS-3 basis set with the additional s-, p-, d-, and f-type , plus g-type functions.

The other Jensen's basis sets, ccJ-pVxZ (x=D–Q) [40], designed specifically for spin-spin coupling constant calculations were tested also. The total change in $\sigma(^{15}\mathrm{N})$ computed by ccJ-pVxZ basis sets is 4.6 ppm (Table 3.1). In terms of number of functions, basis sets ranged from ccJ-pVDZ (105 functions) to ccJ-pVQZ (321 functions). The basis set ccJ-pVTZ predicted -15.6 ppm for $\sigma(^{15}\mathrm{N})$ (similar to the best values by Dunning's basis sets) with only 195 functions. Increasing the to 321 functions (ccJ-pVQZ) resulted in a 0.9 ppm decrease in $\sigma(^{15}\mathrm{N})$.

These studies lead to several conclusions about calculating $\sigma(^{15}\mathrm{N})$ in acetonitrile. The addition of f-type functions on nitrogen does not improve the basis sets convergence (cc-pVTZ value of $\sigma(^{15}\mathrm{N})$ is only lower than that of tzp by 0.3 ppm). Two opposite changes are observed, augmentation of Dunning's basis sets increases $\sigma(^{15}\mathrm{N})$ shielding while adding core functions decreases the shielding. Therefore, the net influence on $\sigma(^{15}\mathrm{N})$ is reflected in aug-cc-pCVXZ. Once we reached the QZ level we get values for $\sigma(^{15}\mathrm{N})$ for the different basis sets in the range of –10.0 to –14.0 ppm. In terms of the cost/accuracy ratio for calculating $\sigma(^{15}\mathrm{N})$, pcS-1 (66 functions) gives a value close to the converged limit. One concludes that Jensen's basis sets converge to the limit with the fewest functions. Finally the remaining error from the experimental value -8.7 ppm [99] (Figure 3.2) could be attributed to the geometric and vibrational effects [102].

3.4 Summary

From Table 3.2, it is concluded that pcS-1 and qz2p basis sets provided a reasonable accuracy for the four nuclei of acetonitrile with the minimal number of functions. The basis set pcS-1 was selected for the MD/QM study in the following chapters.

Table 3.1: **Acetonitrile shielding constants (ppm) calculated at the CCSD//MP2/cc-pVTZ level of theory with various basis sets.**

Basis	^{1}H	$^{13}CH_3$	^{13}CN	^{15}N	Functions
- Dunning -					
cc-pVDZ	30.4	204.2	99.6	22.6	57
cc-pCVDZ	30.4	201.3	94.4	14.8	69
aug-cc-pVDZ	30.3	202.1	95.3	26.0	96
aug-cc-pCVDZ	30.2	199.7	90.7	19.1	108
cc-pVTZ	30.1	194.5	79.5	-7.1	132
cc-pCVTZ	30.1	193.1	77.0	-10.4	171
aug-cc-pVTZ	30.1	194.5	78.6	-3.3	207
aug-cc-pCVTZ	30.0	193.1	76.1	-7.4	246
cc-pVQZ	30.0	192.6	74.8	-10.7	255
cc-pCVQZ	30.0	191.7	73.3	-13.0	342
- Ahlrichs -					
SV(P)	30.8	202.6	96.0	19.0	48
SVP	30.5	202.5	96.5	19.0	57
TZVP	30.4	193.7	77.9	-7.0	111
TZVPP	30.1	193.6	78.1	-7.0	135
QZVP	30.0	192.3	73.7	-11.8	261
- Jensen -					
pcS-0	31.4	200.0	73.1	-31.0	33
pcS-1	30.1	193.6	77.3	-10.5	66
pcS-2	30.1	192.1	72.0	-13.8	141
pcS-3	29.9	191.2	72.0	-13.7	321
ccJ-pVDZ	30.3	192.2	77.2	-19.3	105
ccJ-pVTZ	30.0	191.4	73.3	-15.6	195
ccJ-pVQZ	29.9	191.4	72.5	-14.7	321
- Gauss -					
svp	30.5	202.5	96.0	17.1	57
dzp	30.4	201.5	97.6	20.5	60
tzp	30.6	194.8	79.4	-6.8	75
tz2p	30.3	194.5	78.7	-7.3	99
qz2p	30.3	191.8	74.2	-10.1	114
pz3d2f	30.0	191.6	73.1	-13.5	228
13s9p4d3f	30.0	191.3	72.2	-14.2	324

Table 3.2: **Comparison between pcS-1 and qz2p basis sets used in acetonitrile shielding constants (ppm) calculations at the CCSD/basis//MP2/cc-pVTZ level of theory.**

Basis	^{1}H	$^{13}CH_3$	^{13}CN	^{15}N	Functions
pcS-1	30.1	193.6	77.3	-10.5	66
qz2p	30.3	191.8	74.2	-10.1	114
Conv. Limit (pcS-3)	29.9	191.2	72.0	-13.7	321
Exp.	29.1	187.8	74.0	- 8.9	–

Chapter 4

Comparison of Different Quantum Chemical Methods

The challenge with the methods that treat properly the correlated motion of electrons in molecules is the heavy demands on the computational resources. For example, computations of magnetic shielding constants require the evaluation of the one- and two-electron integrals and their derivatives. The number of the integrals grows with the size of the basis sets employed in the calculations [42]. From the previous chapter, in order to reach the lowest shielding constants values of acetonitrile at least 200 basis functions are needed. In this chapter, we are comparing the accuracy of time efficient methods like DFT (B3LYP and BHandH [106]) and HF to the more expensive and accurate methods (MP2, CCSD, and CCSD(T)) with the Jensen's basis sets (pcS-n) [39].

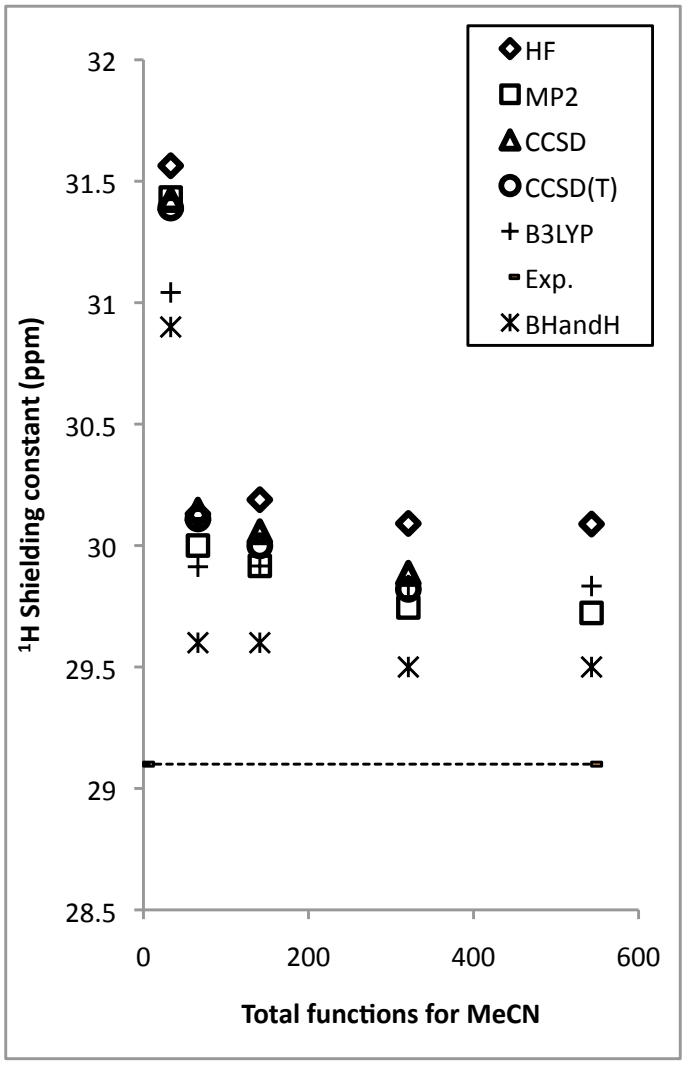

Figure 4.1: Methods used in ^{1}H shielding constant calculations of acetonitrile at the Method/pcS-n//MP2/cc-pVTZ level of theory.

4.1 ^{1}H Shielding Constant

The comparison of different methods was defined by plotting the calculated σ's as a function of the total number of the basis functions, pcS-n (n=0–4), for acetonitrile (Figure 4.1). We used six different methods. All methods showed a sharp change in $\sigma(^1\text{H})$ upon moving form pcS-0 to pcS-1, then a slightly change (0.1–0.3 ppm) from pcS-1 to pcS-4. Convergence of $\sigma(^1\text{H})$ with Jensen's basis sets revealed two significant trends when compared to CCSD

and CCSD(T). HF values were shielded for $\sigma(^1\mathrm{H})$, and MP2 values were deshielded. With pcS-0, B3LYP values $\sigma(^1\mathrm{H})$ were shielded. Then from pcS-1 to pcS-3, B3LYP joined the trend of the coupled-cluster methods. The lowest value (29.5 ppm) produced with BHandH. All the BHandH values were close to the experimental value than those with coupled-cluster methods within the range pcS-1–pcS-3. In conclusion, B3LYP and BHandH provided quite good convergence in computing $\sigma(^1\mathrm{H})$ in acetonitrile.

4.2 ^{13}C Shielding Constants

4.2.1 $^{13}CH_3$ Shielding Constant

The comparison of different methods was defined by plotting the calculated σ's as a function of the total number of the basis functions, pcS-n (n=0–4), for acetonitrile (Figure 4.1). In Figure 4.2 the same electron correlation methods used for $\sigma(^1\mathrm{H})$ are described. All methods showed nice convergence in $\sigma(^{13}\mathrm{CH_3})$ from pcS-0 to pcS-4. Values computed for $\sigma(^{13}\mathrm{CH_3})$ by B3LYP were below the experimental value and quite different from those calculated by the other methods in agreement with a previous study [29] on $\sigma(^{13}\mathrm{CH_3})$ with qz2p basis set. The other DFT method, BHandH, showed a faster convergence towards the experimental value compared to all other methods. Unlike the case with ^{1}H shielding constant HF underestimated and MP2 overestimated the shielding constant with respect to coupled-cluster methods. In conclusion, HF and MP2 produced slightly different values for $\sigma(^{13}\mathrm{CH_3})$ compared to CCSD and CCSD(T) while BHandH was the best method to approach the experimental value 187.8 ppm [99].

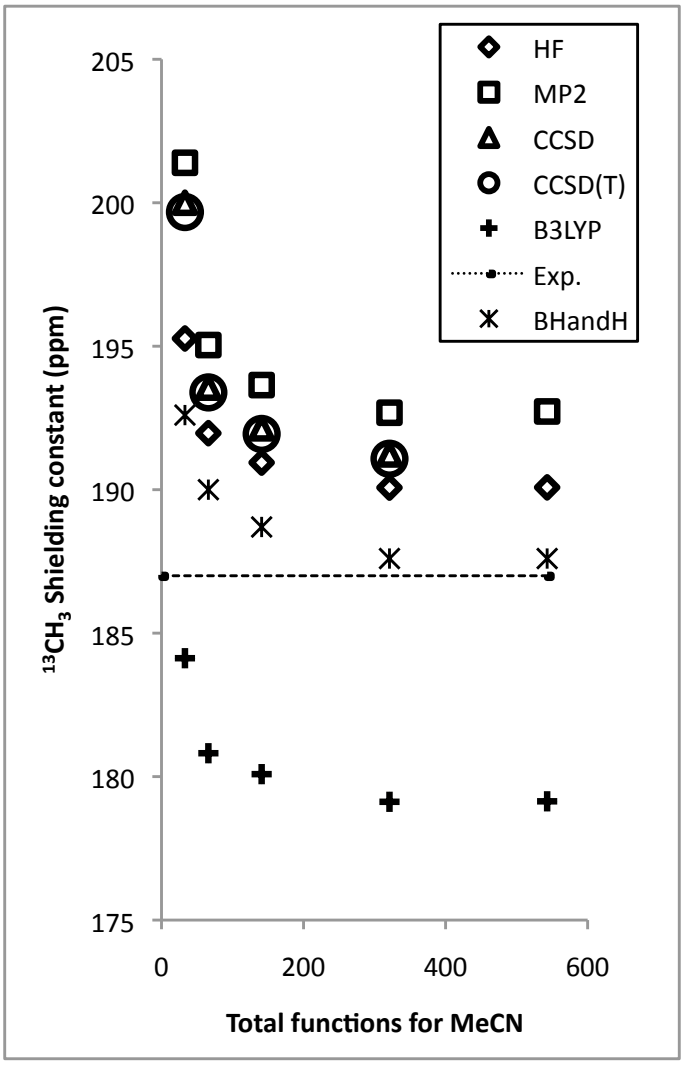

Figure 4.2: Methods used in $^{13}CH_3$ shielding constant calculations of acetonitrile at the Method/pcS-n//MP2/cc-pVTZ level of theory.

4.2.2 ^{13}CN Shielding Constant

The comparison of different methods was defined by plotting the calculated σ's as a function of the total number of the basis functions, pcS-n (n=0–4), for acetonitrile (Figure 4.3). The same methods used for $\sigma(^1H)$ are described Figure 4.3 . All methods showed similar convergence for $\sigma(^{13}CN)$ calculated values from pcS-1 to pcS-4. Values computed for $\sigma(^{13}CN)$ by BHandH, B3LYP, and HF were below the experimental value and quite far from those

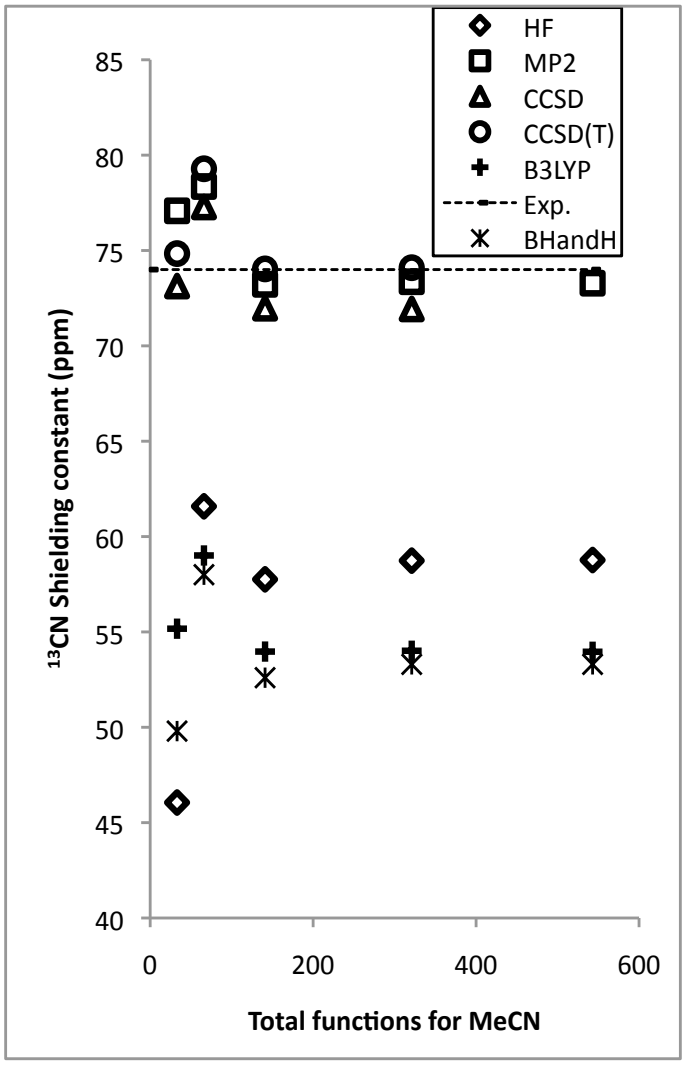

Figure 4.3: Methods used in ^{13}CN shielding constant calculations of acetonitrile at the Method/pcS-n//MP2/cc-pVTZ level of theory.

calculated by the other methods (MP2, CCSD, and CCSD(T)) in agreement with a previous study [29] with qz2p basis set for HF and B3LYP. Unlike the case with $\sigma(^1\text{H})$, HF values for $\sigma(^{13}\text{CN})$ were deshielded and MP2 were shielded with respect to coupled-cluster methods. In conclusion, MP2 produced slightly different values for $\sigma(^{13}\text{CN})$ with those computed at the coupled-cluster level, while HF and DFT methods produced larger errors from the experimental value 74.0 ppm [99].

4.3 ^{15}N Shielding Constant

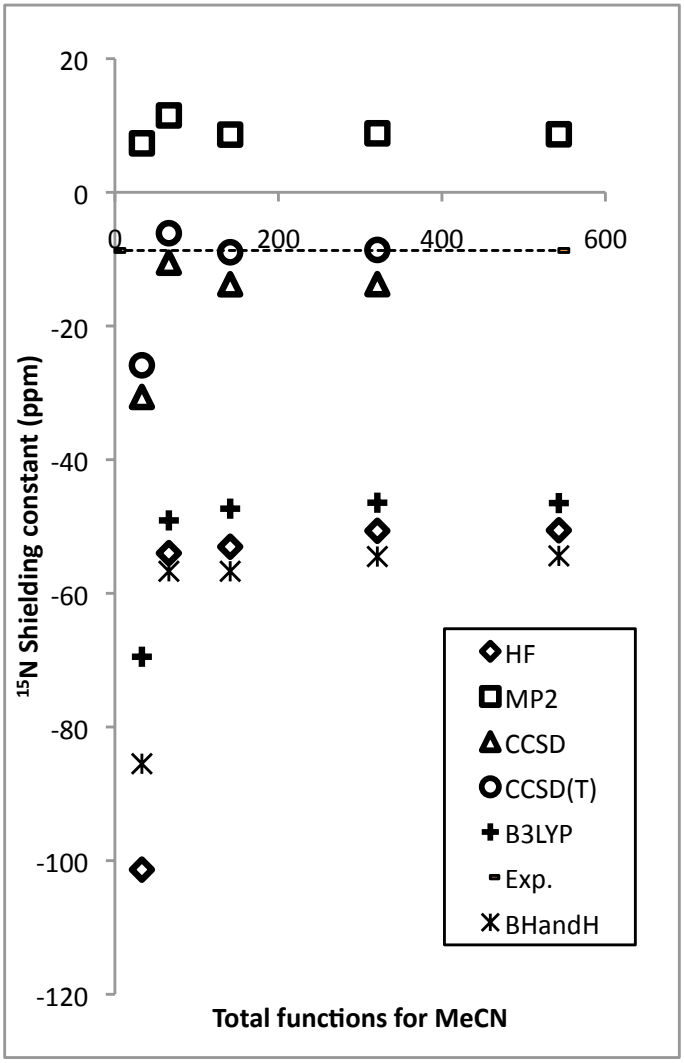

Figure 4.4: Methods used in ^{15}N shielding constant calculations of acetonitrile at the Method/pcS-n//MP2/cc-pVTZ level of theory.

The comparison of different methods was defined by plotting the calculated σ's as a function of the total number of the basis functions, pcS-n (n=0–4), for acetonitrile (Figure 4.4). The same methods used for $\sigma(^{1}\mathrm{H})$ are described Figure (4.4). All methods showed similar convergence to that seen for $\sigma(^{13}\mathrm{CN})$ calculated values from pcS-1 to pcS-4. The values calculated with pcS-0 were lower than the others basis sets. No significant change in $\sigma(^{15}\mathrm{N})$

was observed by moving from pcS-2 to pcS-3. MP2 values of $\sigma(^{15}\mathrm{N})$ were positive with all pcS-n basis sets. Compared to other methods, CCSD and CCSD(T), approached the experimental value –8.7 ppm [99], only after the pcS-0 basis set. CCSD(T) method had a minor effect on the calculated shielding constant in comparison to the CCSD method. In conclusion, the calculation of $\sigma(^{15}\mathrm{N})$ in acetonitrile, triple bond nitrogen, required the treatment at the coupled-cluster level [102].

4.4 Summary

BHandH/pcS-1 level of theory compared to a higher accurate level (CCSD(T)/pcS-3) provided reasonable accuracy for shielding constants of singly bonded nuclei in acetonitrile ($^{1}\mathrm{H}$ and $^{13}\mathrm{CH_3}$) while triple-bonded nuclei ($^{13}\mathrm{CN}$ and $^{15}\mathrm{N}$) required the treatment at the coupled-cluster level Table 4.2.

Table 4.1: **Acetonitrile shielding constants (ppm) calculated by different quantum chemical methods at the Method/pcS-n//MP2/cc-pVTZ level of theory.**

Nucleus	HF	MP2	CCSD	CCSD(T)	B3LYP	BHandH
- ^{1}H -						
pcS-0	31.6	31.4	31.4	31.4	31.0	30.9
pcS-1	30.1	30.0	30.1	30.1	29.9	29.6
pcS-2	30.2	29.9	30.1	30.0	29.9	29.6
pcS-3	30.1	29.7	29.9	29.8	29.8	29.5
pcS-4	30.1	29.7	-	-	29.8	29.5
Exp.				29.1		
- ^{13}CH$_3$ -						
pcS-0	195.3	201.4	200.0	199.7	184.1	192.6
pcS-1	192.0	195.0	193.6	193.4	180.8	190.0
pcS-2	190.9	193.6	192.1	191.9	180.1	188.7
pcS-3	190.1	192.7	191.2	191.1	179.1	187.6
pcS-4	190.1	192.7	-	-	179.1	187.6
Exp.				187.8		
- ^{13}CN -						
pcS-0	46.1	77.1	73.1	74.8	55.2	49.8
pcS-1	61.6	78.4	77.3	79.3	59.0	58.0
pcS-2	57.8	73.2	72.0	74.0	54.0	52.6
pcS-3	58.7	73.4	72.0	74.1	54.0	53.3
pcS-4	58.8	73.3	-	-	54.0	53.3
Exp.				74.0		
- ^{15}N -						
pcS-0	-101.3	7.3	-30.6	-25.9	-69.5	-85.5
pcS-1	-54.0	11.5	-10.5	-6.1	-49.1	-56.7
pcS-2	-53.0	8.6	-13.8	-9.0	-47.3	-56.0
pcS-3	-50.6	8.8	-13.7	-8.6	-46.4	-54.5
pcS-4	-50.6	8.7	-	-	-46.5	-54.4
Exp.				-8.9		

Table 4.2: **Comparison of methods/pcS-1//MP2/cc-pVTZ on computed shielding constants for acetonitrile with CCSD(T)/pcS-3//MP2/cc-pVTZ.**

Nucleus	^{1}H	$^{13}CH_3$	^{13}CN	^{15}N
HF	30.1	192.0	61.6	-54.0
MP2	30.0	195.0	78.4	11.5
CCSD	30.1	193.6	77.3	-10.5
B3LYP	29.9	180.8	59.0	-49.1
BHandH	29.6	190.0	58.0	-56.7
CCSD(T)/pcS-3	29.8	191.1	74.1	-8.6
Exp.	29.1	187.7	74.0	-8.9

Chapter 5

Nuclear Contributions to the Nuclear Shielding Constants

5.1 Molecular Vibrations

To predict the experimental values of molecular properties, vibrational corrections must be included [107]. In this chapter, the contributions of molecular vibrations to the nuclear magnetic shielding constants of acetonitrile were investigated. The approach is based on the vibrational perturbation theory [108]. The procedure required shielding constant calculations for the input and displaced geometries, evaluation of harmonic frequencies and cubic force constants, followed by the first- and second-order differentiation of the shielding constants with respect to the normal coordinates.

Vibrational corrections to the shielding constants (Table 5.1) of the different nuclei of acetonitrile calculated at the HF level with Dunning's basis sets. The values in the table showed significant differences among the nuclei. The corrections varied from –0.3 ppm to –6.0 ppm

Table 5.1: **Vibrational corrections (ppm) to acetonitrile shielding constants at the HF/cc-pVxZ and HF/aug-cc-pVxZ levels of theory.**

Basis	^{1}H	$^{13}CH_3$	^{13}CN	^{15}N
cc-pVDZ	–0.332	–1.255	–1.562	–6.237
cc-pCVDZ	–0.328	–1.053	–1.562	–6.237
aug-cc-pVDZ	–0.357	–1.123	–1.519	–6.197
aug-cc-pCVDZ	–0.347	–0.999	–1.585	–6.152
cc-pVTZ	–0.303	–1.112	–1.414	– 5.887
cc-pCVTZ	–0.316	–1.078	–1.476	–6.034
aug-cc-pVTZ	–0.315	–1.190	–1.371	–5.978
aug-cc-pCVTZ	–0.321	–1.100	–1.459	–6.063
cc-pVQZ	–0.315	–1.127	–1.364	–6.029

for the different nuclei in acetonitrile which is proportional to the shielding range for each [109]. Basis sets had small effect on the vibrational correction values. All the vibrational corrections were negative; in other words, the vibrations of the molecule deshielded the nuclei [29] [102].

The vibrational correction to $\sigma(^{1}H)$ in acetonitrile was $\sim$ –0.3 ppm. Ruud et al. [104] studied vibrational corrections to $\sigma(^{1}H)$ on 40 different organic molecules and the range varied from –0.2 to –0.7 ppm. The –0.3 ppm correction reduced the error for all the methods (Figure 4.1). The best theoretical value (29.5 ppm), BHandH/pcS-3, differed by 0.1 ppm from the experimental value (29.1 ppm) [99] with the vibrational correction.

For $\sigma(^{13}CH_3)$, the vibrational correction varied from –1.0 to –1.3 ppm. At the MP2 level [29], the vibrational correction to $\sigma(^{13}CH_3)$ was –2.4 ppm. This correction increased the error in any prediction made with B3LYP (Figure 4.2). While with BHandH, error increased with the extended basis sets, pcS-3 and pcS-4. For the ab initio methods, the error reduced by $\sim$ 25–50 % for $\sigma(^{13}CH_3)$ with the vibrational corrections.

For $\sigma(^{13}CN)$, the vibrational correction varied from –1.4 to –1.6 ppm. At the MP2 level [29], the vibrational correction to $\sigma(^{13}CN)$ was –1.5 ppm. The vibrational corrections increased

the error for HF, BHandH, and B3LYP methods (Figure 4.3). in predicting the experimental value. While it reduced the error for MP2 with pcS-0 and pcS-1, for CCSD and CCSD(T) with pcS-1 basis set. Then from pcS-2 to pcS-4 the error increased.

For $\sigma(^{15}\mathrm{N})$, the vibrational corrections was $\sim$ –6.0 ppm. At the MP2 and CCSD(T) levels for HCN molecule [102], the vibrational corrections to $\sigma(^{15}\mathrm{N})$ were –5.2 and –8.2 ppm respectively. The vibrational corrections increased the error for HF, BHandH, and B3LYP methods (Figure 4.4). For MP2 values the error reduced upon vibrational corrections. The predicted values by CCSD and CCSD(T) along pcS-1–pcS-3 were close to the experimenatl value of $\sigma(^{15}\mathrm{N})$ and with the vibrational correction, the error increased.

5.2 Molecular Geometry

To compute any molecular property, an equilibrium molecular geometry is required. Equilibrium molecular geometries (r_e) can now be determined accurately with electronic structure methods [110]. This theoretical molecular structure is obtained as an isolated molecule at 0 K and without any vibrational motions involved (no vibrational averaging); in other words, at the minimum of the potential energy surface. There are other ways to describe molecular structures. The effective molecular structure (r_0) is derived from the rotational constants of the ground vibrational states of the molecule. The substitution structure (r_s) is derived from the shifts in rotational constants due to isotopic substitution [111].

The structure of acetonitrile has been studied extensively by experimental methods, by microwave spectroscopy [93] [112] [113], by gas electron diffraction [114], by NMR [115] as well as by theoretical methods [116] [117].

The geometric structure of acetonitrile is usually described with four parameters: CH, CC,

and CN bond lengths, and CCH bond angle. In the following study, the equilibrium structure (MP2/cc-pVTZ) of acetonitrile was altered with geometrical parameters from the substitution and effective structures [93]. The effect of distorted geometry on the nuclear magnetic shielding constants was investigated. The result of four geometric parameters and four nuclei is sixteen. Only two of them were significant (Figures 5.1–5.4). All the shielding constants calculations have been performed at the CCSD/pcS-1 and BHandH/pcS-1 levels of theory.

Table 5.2: **The r_e, r_s, and r_0 structures of acetonitrile.**

Structure	CH bond ($\AA$)	CN bond ($\AA$)	CC bond ($\AA$)	HCC angle
r_e	1.08573	1.15573	1.45850	109.9 °
r_s	1.10250	1.15710	1.45836	109.5 °
r_0	1.11200	1.15720	1.45820	109.6 °

In Figures 5.1–5.4, ^{1}H and $^{13}CH_3$ shielding constants are plotted versus the change in C-H bond length and the rest of the geometrical parameters were kept constant. The values used for the C-H bond length are from the r_e, r_s, and r_0 structures (Table 5.2). Moving from the shortest to the longest C-H bond length, the $^{13}CH_3$ shielding constant changed by $\sim$ 3.5 ppm. Smaller effects , not shown, were observed for ^{13}CN and ^{15}N shielding constants, $\sim$ 0.03 and $\sim$ 0.04 ppm respectively. The change in ^{1}H shielding constant ($\sim$ 0.8 ppm) is not negligible due to the small range spanned by proton chemical shift. In both cases, these changes brought calculated shielding closer to experimental values.

5.3 Summary

In conclusion, the nuclear motion can change the value of the shielding constant either by manually modifying the geometry or by molecular vibration. Different nuclei have different vibrational contributions to the shielding constants. All vibrational corrections are in the deshield direction. Therefore, in cases where the predicted value for σ is below the

experimental one, the error will increase.

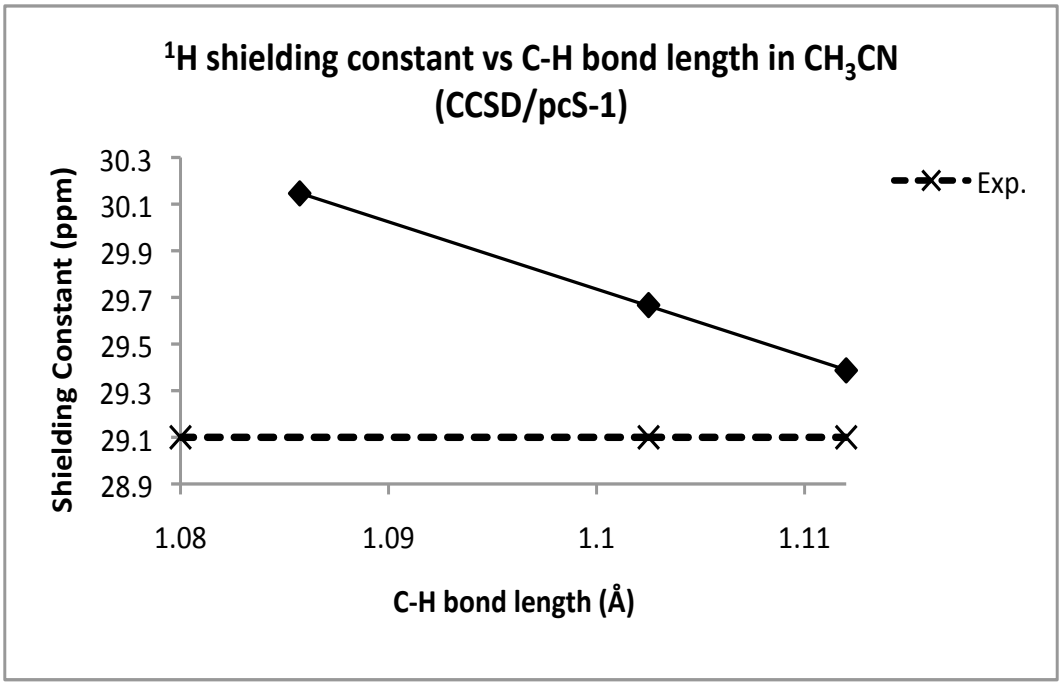

Figure 5.1: The effect of change of C-H bond length on the ^{1}H shielding constant of acetonitrile at CCSD/pcS-1 level.

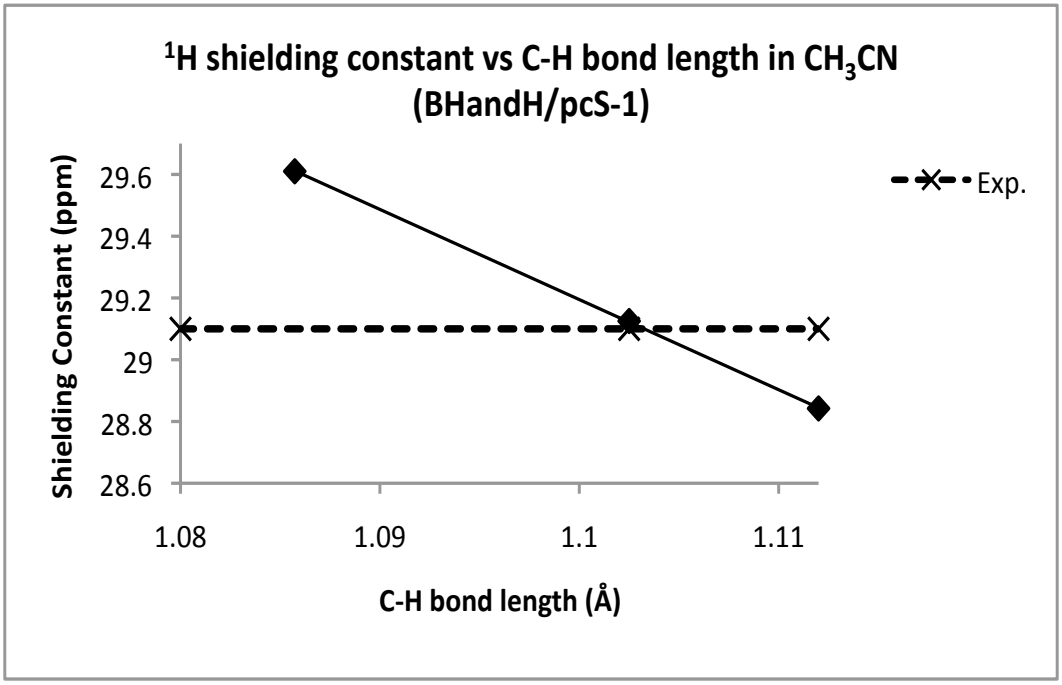

Figure 5.2: The effect of change of C-H bond length on the ^{1}H shielding constant of acetonitrile at BHandH/pcS-1 level.

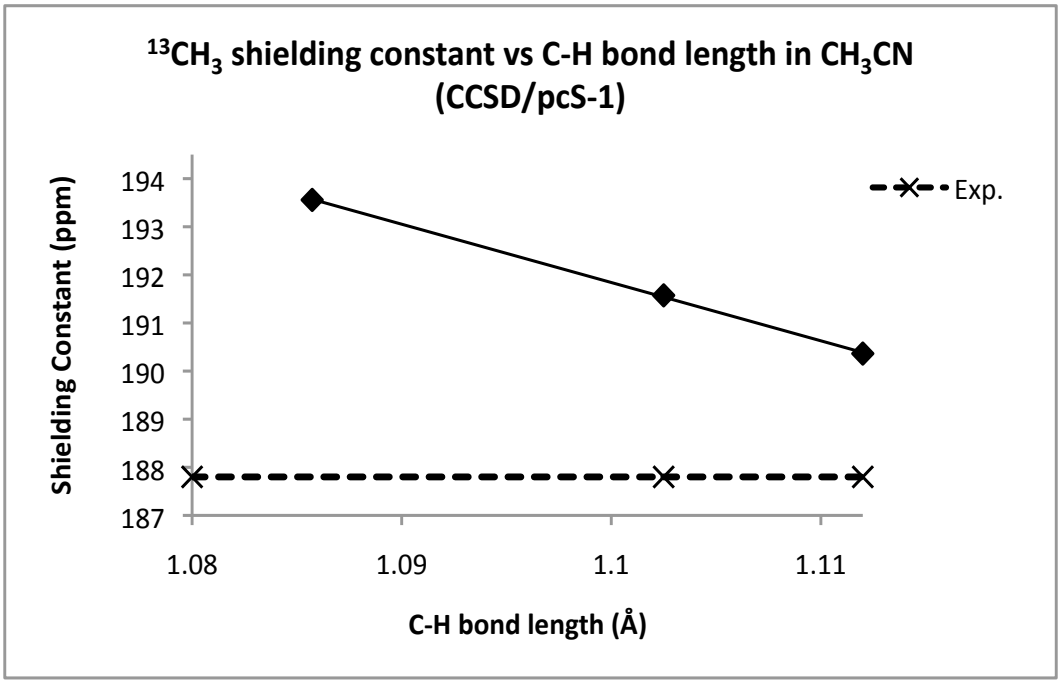

Figure 5.3: The effect of change of C-H bond length on the $^{13}CH_3$ shielding constant of acetonitrile at CCSD/pcS-1 level.

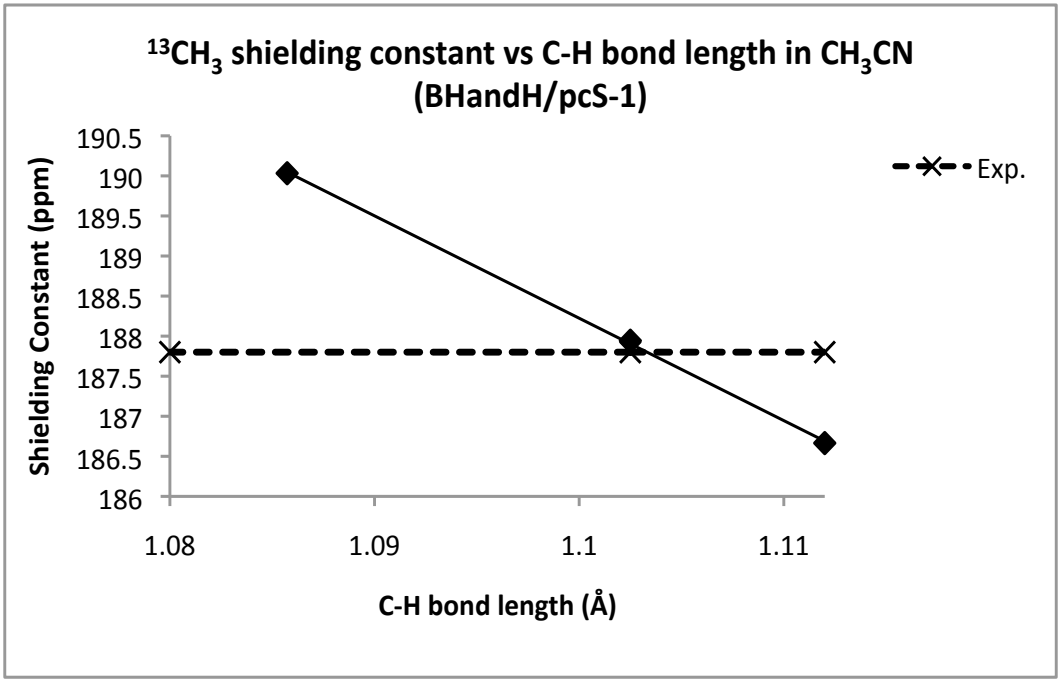

Figure 5.4: The effect of change of C-H bond length on the $^{13}CH_3$ shielding constant of acetonitrile at BHandH/pcS-1 level.

Chapter 6

Predicting Acetonitrile Shielding Constants in the Liquid Phase

6.1 Gas to Liquid Shift

There is a difference in the values of the nuclear magnetic shielding constants of acetonitrile from the gas phase to the liquid phase. A gas to liquid shift (in ppm) of –0.7, –5.0, –7.8, and 9.8 for $\sigma(^{1}\mathrm{H})$, $\sigma(^{3}\mathrm{CH_3})$, $\sigma(^{13}\mathrm{CN})$, and $\sigma(^{15}\mathrm{N})$ respectively, occurs [99]. The prediction of this difference is not trivial. Liquids do not have random structure like gases or well-ordered structure like solids; but a mix of both, order and disorder structures [118]. This structural complexity represents a challenge to study liquids. An interpretation of liquid properties based only on experimental data is difficult. Computer simulation can lessen this difficulty. There are different computational methods to predict the shielding constants of liquids; continuum models [75], molecular dynamics (MD) simulations [119], and Car-Parrinello simulations [120].

6.2 Molecular Dynamics Simulations

MD simulations is a well founded technique to study liquids at the molecular level. In this chapter, we used MD simulation in combination with quantum chemistry to model the shielding constants of liquid acetonitrile. Different clusters were extracted from the MD simulations (see below), to investigate the cluster environment and cluster size on the calculated shielding constants.

In our study, MD simulations were done for liquid acetonitrile with the TINKER program [121]. The computational cell (cubic box), of 729 acetonitrile molecules (Figure 6.1), was first created with the MOLDEN program [122]. The OPLS [123] force field was applied in simulation. First, the simulation was run with the NVT ensemble with a temperature of 1000 K for 500 ps. Then an annealing process was performed for another 500 ps to achieve a temperature of 298 K. This was followed by an equilibration (Figure 6.2) with the NPT ensemble for 500 ps. No further change in the density after the 500.0 ps. From the final results of the simulations we chose nine different clusters of molecules. A molecule was selected as the center of each cluster. One cluster near the center and another eight were in the surroundings octants, a combination of positive and negative directions of the xyz coordinates (Table 6.1) around the central cluster.

The size of the selected clusters was based on the radial distribution function (RDF) [124]. The RDF was defined as the distance between the center of masses of acetonitrile.The RDF was built by the RADIAL module in the TINKER program. There are two peaks in the RDF, the so-called first and second solvation shells (Figures 6.3a – 6.11a). The peaks for the first solvation shell was ~ 4.5 $\mathring{A}$; the peak of the second solvation shell was ~ 8.0 $\mathring{A}$. The number of molecules within 6.0 $\mathring{A}$ (the cutoff distance for the first solvation shell) varied, 6–10, for each cluster. Extending the distance to the second solvation shell brings the cluster

size to 20 molecules. The initial intention was to include only the molecules within the first solvation shell in our calculations of the shielding constants, but an extension to 15 molecules for each cluster was required to assure the convergence of the shielding constants.

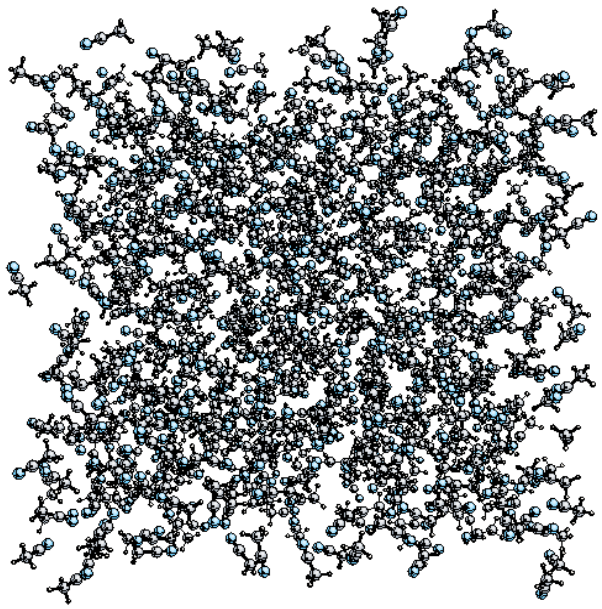

Figure 6.1: A box of 729 acetonitrile molecules used in the MD simulation.

6.3 Shielding Constants in the Liquid Phase

In Figures (6.3a – 6.11a), the RDF (y-axis 1) and the number of molecules (y-axis 2) were plotted versus the distance of each molecule in the cluster from the central molecule (x-axis). The number and distribution of molecules varied with the distance from the central molecule in each cluster. For example, seven molecules are in the first solvation shell (≤ 6 $\mathring{A}$) of the center cluster (Figure 6.11a) while there are ten molecules for cluster three (Figure 6.5a). In cluster eight (Figure 6.10a), where four molecules were at the same distance from the central molecule.

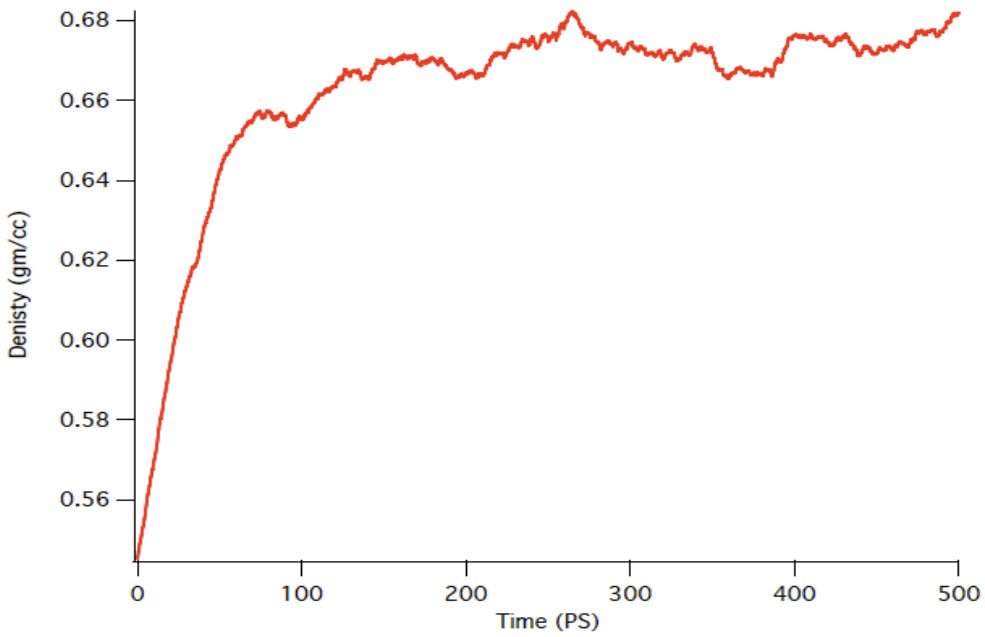

Figure 6.2: Density of acetonitrile from MD simulation.

Extracting clusters from MD simulations to predict the shielding constants of liquid acetonitrile raised several questions. How does the distribution of molecules in a cluster affect the shielding constants of the central molecule? How many molecules should be included in a cluster to reach convergence of the calculated shielding constants? Is there is a connection between the RDF and the convergence of $\sigma(^{1}\mathrm{H})$ and $\sigma(^{13}\mathrm{CH_3})$? What is the role of the geometry of the investigated molecule in the cluster and the calculated σs? We will try to answer these questions in the following sections.

In Figures (6.3b – 6.11b) and (6.3c – 6.11c) respectively, calculated $\sigma(^{1}\mathrm{H})$ and $\sigma(^{13}\mathrm{CH_3})$ of the central molecule in the different nine clusters were plotted versus the increase in the number of molecules at the BHandH/pcS-1 level of theory. Shielding constants, $\sigma(^{13}\mathrm{CN})$ and $\sigma(^{15}\mathrm{N})$, were ignored because BHandH failed to provide reasonable results for these triple bonded nuclei in the gas phase. The geometries of CH_3CN molecules produced from MD simulations were not optimum. To investigate the role of geometry. Two different curves

Table 6.1: **The positions of nine clusters of acetonitrile with respect to the origin of the cubic box used in the MD simulations, and corresponding figure numbers for RDF, $\sigma(^1H)$, $\sigma(^{13}CH_3)$, and the distance of nearest neighbor (d).**

Cluster	X	Y	Z	RDF	$\sigma(^1H)$	$\sigma(^{13}CH_3)$	d ($\mathring{A}$)
One	–	–	–	6.3a	6.3b	6.3c	3.7
Two	–	+	–	6.4a	6.4b	6.4c	3.4
Three	+	+	–	6.5a	6.5b	6.5c	3.8
Four	+	–	–	6.6a	6.6b	6.6c	4.0
Five	–	–	+	6.7a	6.7b	6.7c	3.7
Six	–	+	+	6.8a	6.8b	6.8c	3.2
Seven	+	+	+	6.9a	6.9b	6.9c	3.4
Eight	+	–	+	6.10a	6.10b	6.10c	4.1
Center	~ 0	$\sim$0	$\sim$0	6.11a	6.11b	6.11c	3.5

were plotted in each graph. The first curve represents the original MD cluster; the second curve represents the same cluster but with the geometry of the central molecule modified to the r_0 geometry of CH_3CN [93].

For $\sigma(^1H)$ in all clusters the shapes of the two curves are similar; with the r_0 curves below the MD curves except for cluster seven Figure (6.9b), they are nearly matched. While for $\sigma(^{13}CH_3)$ the r_0 curves below the MD curves except for cluster seven Figure (6.9c) the reverse is correct and cluster eight Fig (6.10c) the two curves are close. One concluded from these cases the significant role of the starting geometry of the central molecule in a cluster. The starting shielding constant values for each cluster differed, and this is because of the molecular geometry of the central molecule in each cluster is different.

The distribution of each cluster played a role in the range of change of the shielding constants of the central molecule. It is small as 0.1 ppm for cluster eight or large as 0.7 ppm for cluster six regrading $\sigma(^1H)$. It is small as 0.6 ppm for center cluster or large as 7.9 ppm for cluster two regrading $\sigma(^{13}CH_3)$. Different distributions produced different curves of the change of shielding constants with the size of each cluster.

The connection between the required number of molecules to reach convergence and the number extracted from the first solvation shell in the RDF Figures (6.3a – 6.11a) is not related, unpredictable. For example, two molecules only ($\sigma(^{13}CH_3)$ in cluster one) are required to reach convergence while there are nine molecules within the first solvation shell, RDF figure (6.3a). Another example, eleven molecules ($\sigma(^{13}CH_3)$ in cluster seven) were required to reach convergence while there are nine molecules within the first solvation shell, RDF figure (6.9a). What is observed for $\sigma(^{1}H)$ in all clusters is that the number of molecules required to reach convergence is always lower than the one from RDFs under the first solvation shell.

In Figures 6.12 and 6.13 respectively, the average change in $\sigma(^{1}H)$ and $\sigma(^{13}CH_3)$ in the central molecules of the different nine clusters of acetonitrile were plotted versus the size of the clusters at the BHandH/pcS-1 level. The convergence towards the experimental values is now smooth and achieved with the minimum number of molecules. The same behavior was observed for $\sigma(^{13}CN)$ and $\sigma(^{15}N)$, Figures 6.14 and 6.15 respectively.

6.4 Summary

The shape and size of a cluster played a role in the values of $\sigma(^{1}H)$ and $\sigma(^{13}CH_3)$ of acetonitrile in the liquid phase. However, the geometry of the central molecule in a cluster is a significant factor in converging to the experimental values, Figures 6.12 and 6.13.

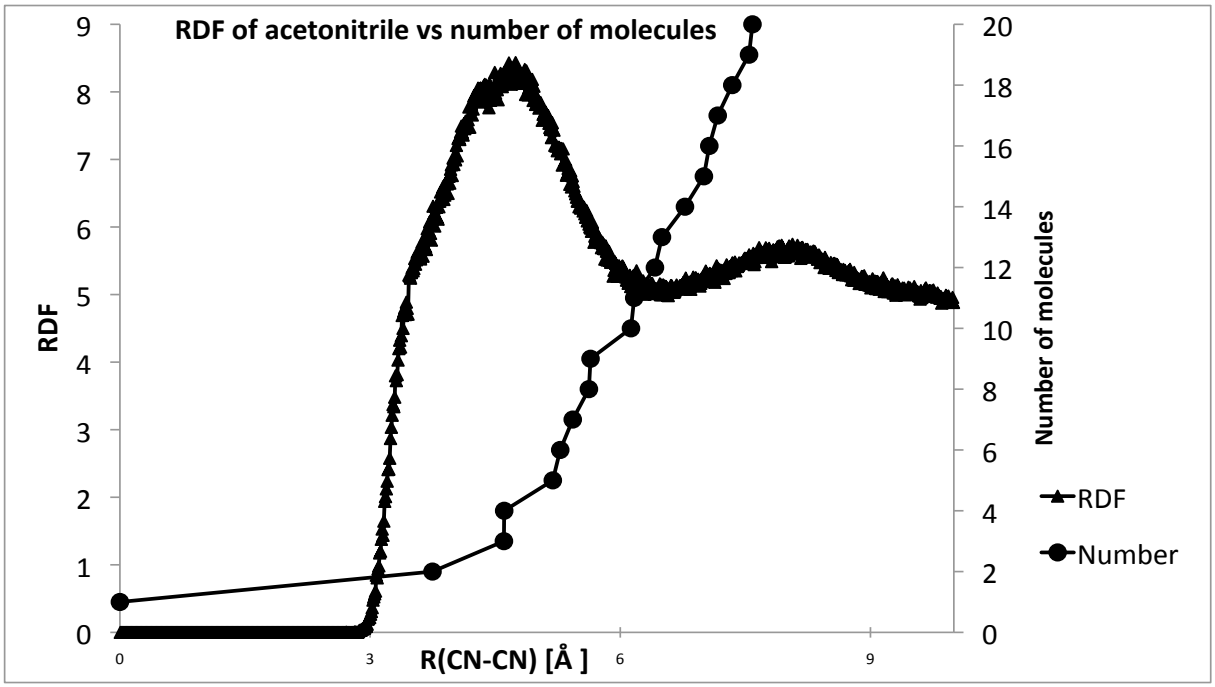

(a) RDF

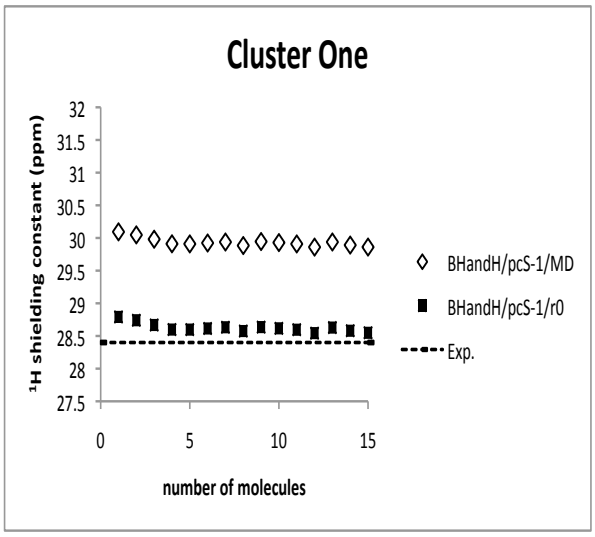

(b) $\sigma(^1\mathrm{H})$

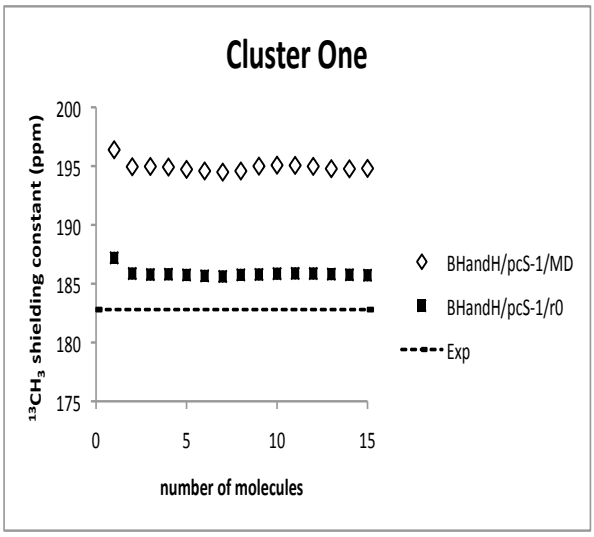

(c) $\sigma(^{13}\mathrm{CH_3})$

Figure 6.3: (a) The radial distribution function (left) of acetonitrile and the number of molecules (right) versus the distance from the central molecule in cluster one. (b) The change in $\sigma(^1\mathrm{H})$ of the central molecule versus the size of the cluster of acetonitrile at the BHandH/pcS-1 level. (c) The change in $\sigma(^{13}\mathrm{CH_3})$ of the central molecule versus the size of the cluster of acetonitrile at the BHandH/pcS-1 level.

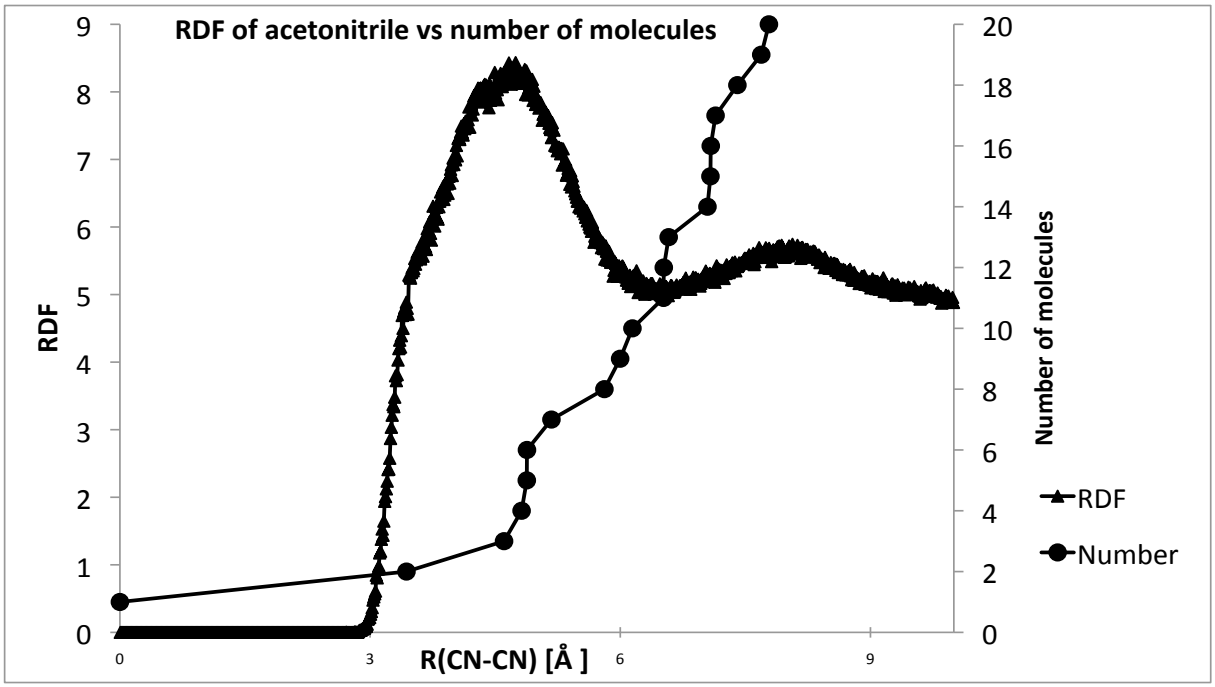

(a) RDF

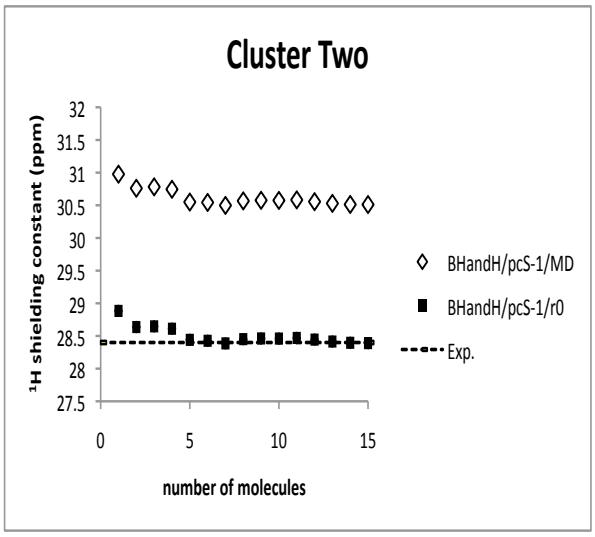

(b) $\sigma(^1\mathrm{H})$

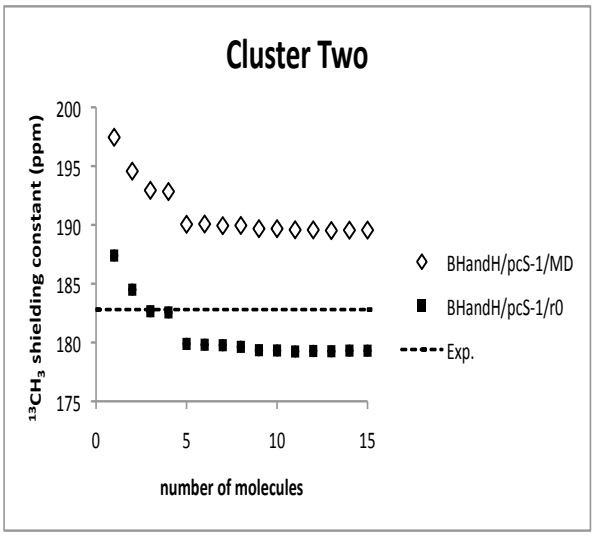

(c) $\sigma(^{13}\mathrm{CH_3})$

Figure 6.4: (a) The radial distribution function (left) of acetonitrile and the number of molecules (right) versus the distance from the central molecule in cluster two. (b) The change in $\sigma(^1\mathrm{H})$ of the central molecule versus the size of the cluster of acetonitrile at the BHandH/pcS-1 level. (c) The change in $\sigma(^{13}\mathrm{CH_3})$ of the central molecule versus the size of the cluster of acetonitrile at the BHandH/pcS-1 level.

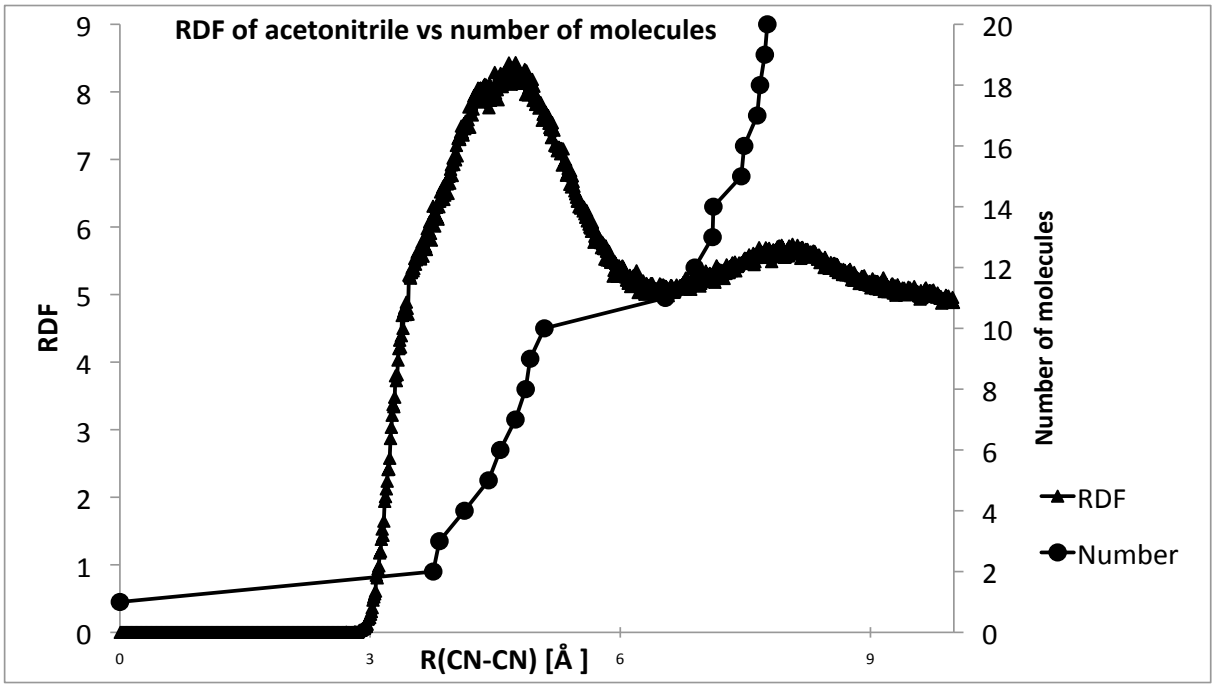

(a) RDF

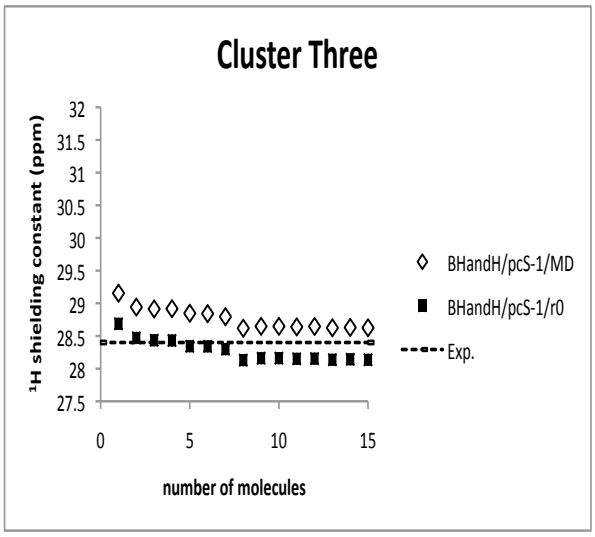

(b) $\sigma(^1\mathrm{H})$

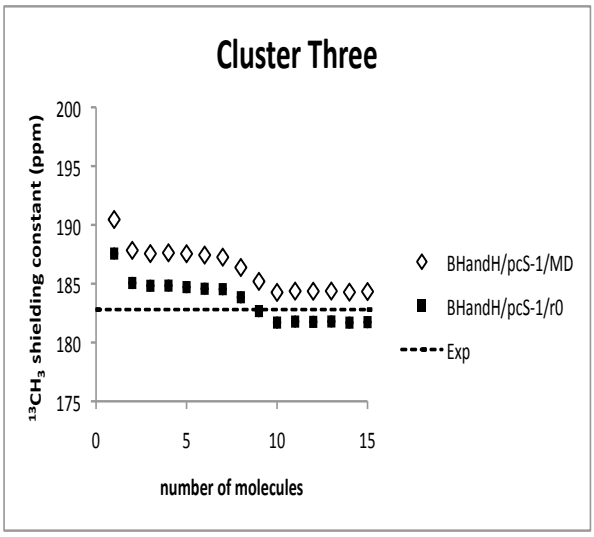

(c) $\sigma(^{13}\mathrm{CH_3})$

Figure 6.5: (a) The radial distribution function (left) of acetonitrile and the number of molecules (right) versus the distance from the central molecule in cluster three. (b) The change in $\sigma(^1\mathrm{H})$ of the central molecule versus the size of the cluster of acetonitrile at the BHandH/pcS-1 level. (c) The change in $\sigma(^{13}\mathrm{CH_3})$ of the central molecule versus the size of the cluster of acetonitrile at the BHandH/pcS-1 level.

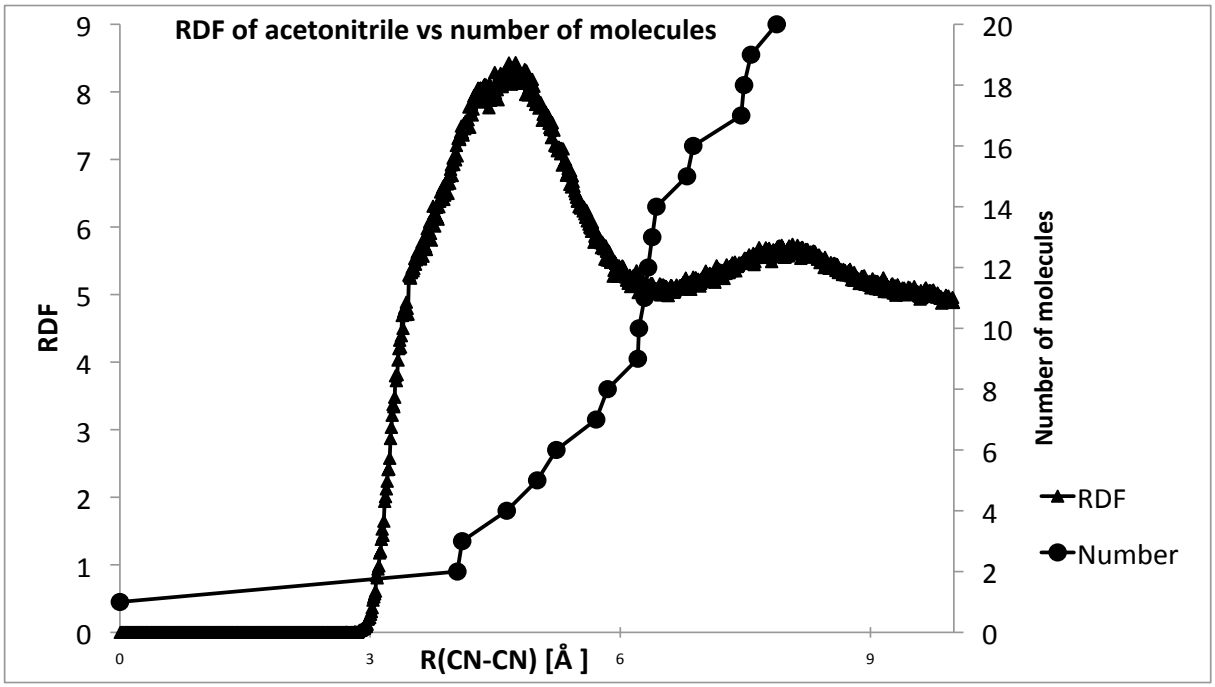

(a) RDF

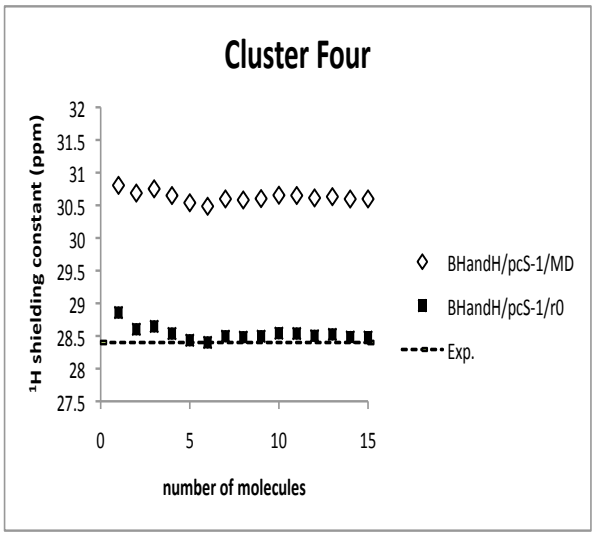

(b) $\sigma(^1\mathrm{H})$

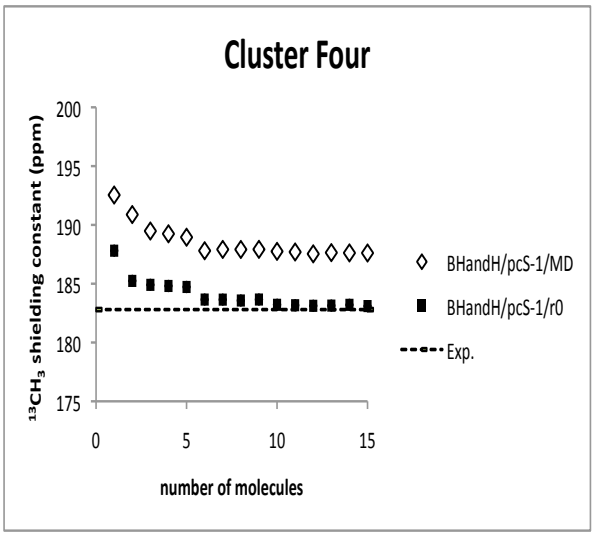

(c) $\sigma(^{13}\mathrm{CH_3})$

Figure 6.6: (a) The radial distribution function (left) of acetonitrile and the number of molecules (right) versus the distance from the central molecule in cluster four. (b) The change in $\sigma(^1\mathrm{H})$of the central molecule versus the size of the cluster of acetonitrile at the BHandH/pcS-1 level. (c) The change in $\sigma(^{13}\mathrm{CH_3})$ of the central molecule versus the size of the cluster of acetonitrile at the BHandH/pcS-1 level.

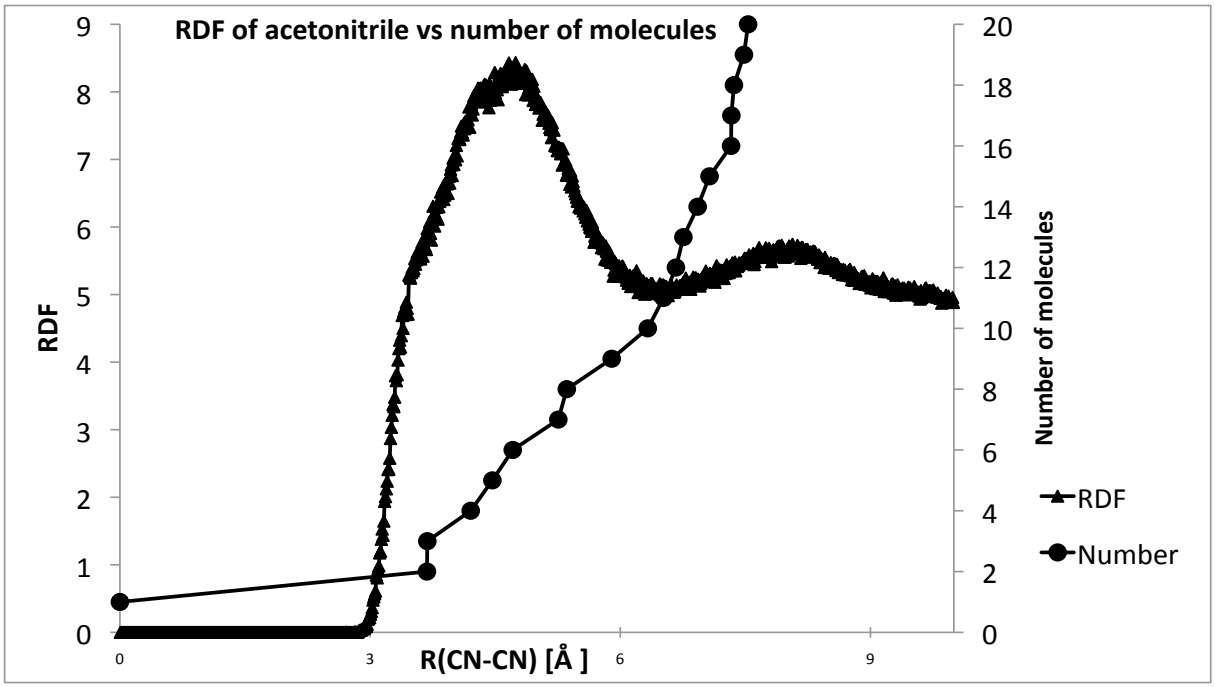

(a) RDF

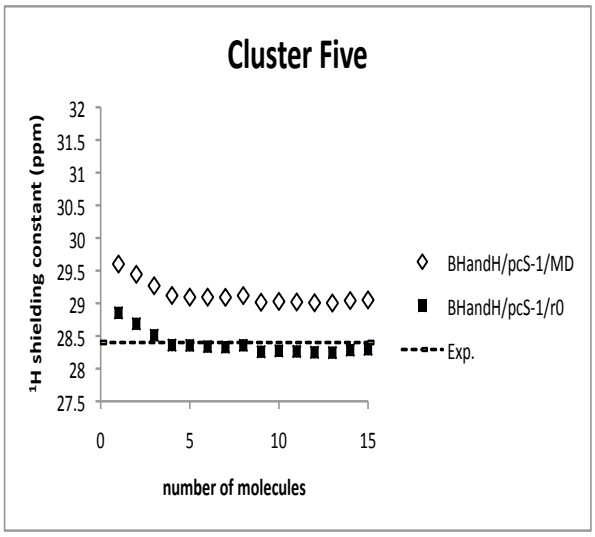

(b) $\sigma(^1\mathrm{H})$

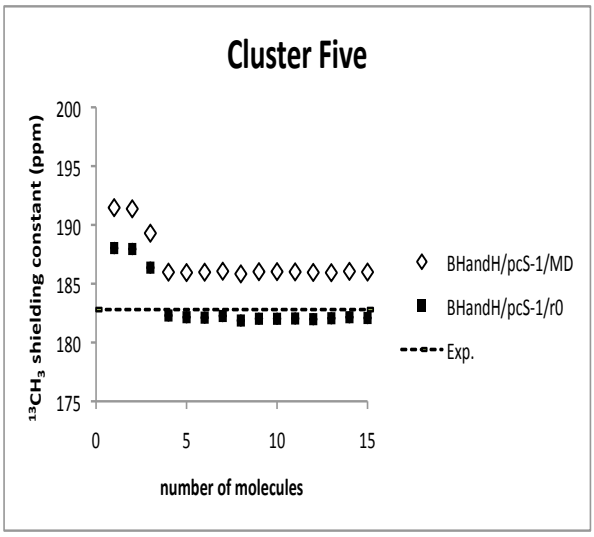

(c) $\sigma(^{13}\mathrm{CH_3})$

Figure 6.7: (a) The radial distribution function (left) of acetonitrile and the number of molecules (right) versus the distance from the central molecule in cluster five. (b) The change in $\sigma(^1\mathrm{H})$ of the central molecule versus the size of the cluster of acetonitrile at the BHandH/pcS-1 level. (c) The change in $\sigma(^{13}\mathrm{CH_3})$ of the central molecule versus the size of the cluster of acetonitrile at the BHandH/pcS-1 level.

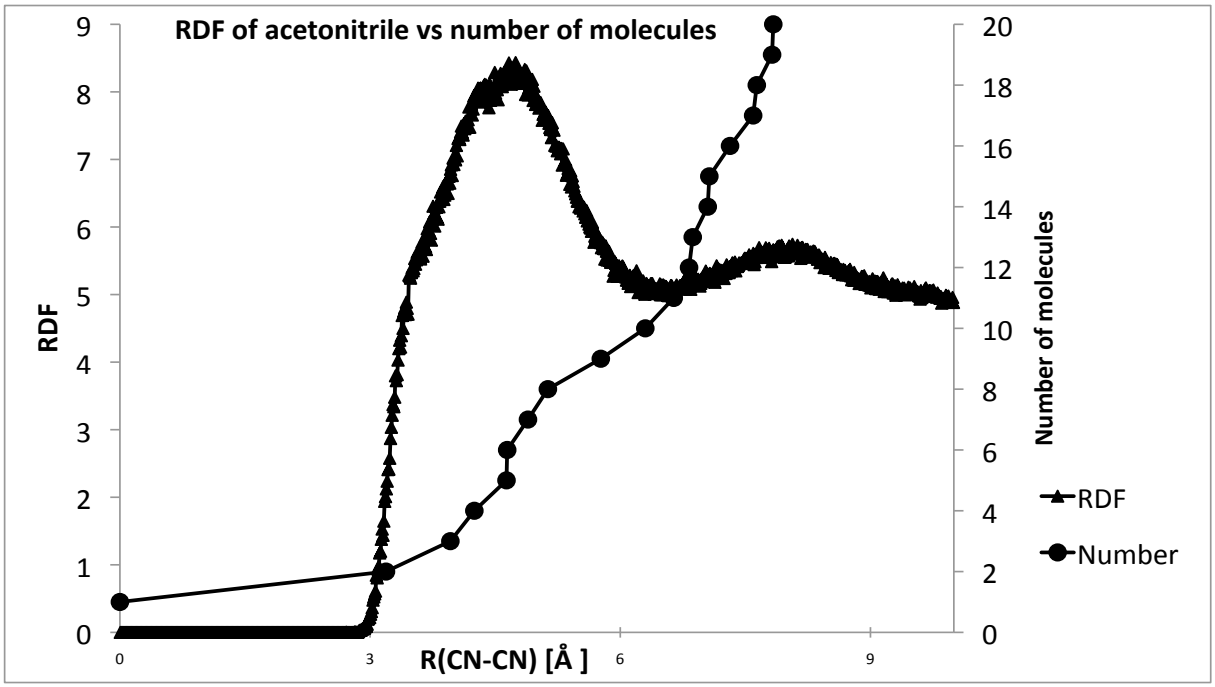

(a) RDF

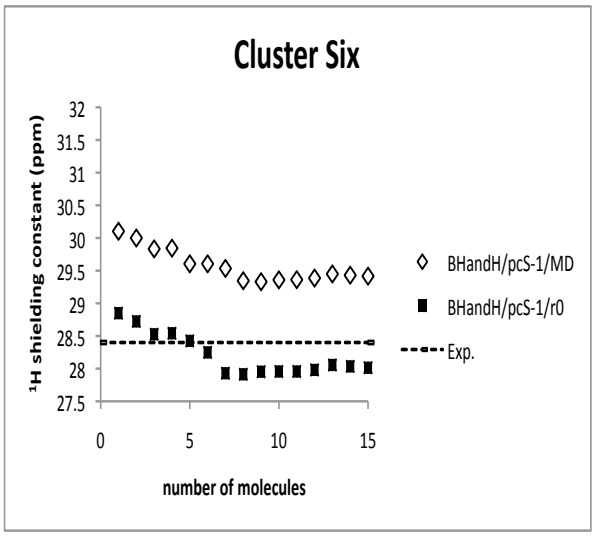

(b) $\sigma(^1\mathrm{H})$

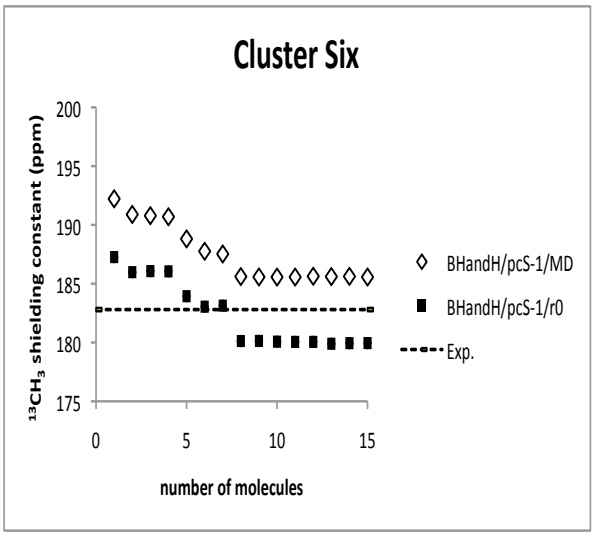

(c) $\sigma(^{13}\mathrm{CH_3})$

Figure 6.8: (a) The radial distribution function (left) of acetonitrile and the number of molecules (right) versus the distance from the central molecule in cluster six. (b) The change in $\sigma(^1\mathrm{H})$ of the central molecule versus the size of the cluster of acetonitrile at the BHandH/pcS-1 level. (c) The change in $\sigma(^{13}\mathrm{CH_3})$ of the central molecule versus the size of the cluster of acetonitrile at the BHandH/pcS-1 level.

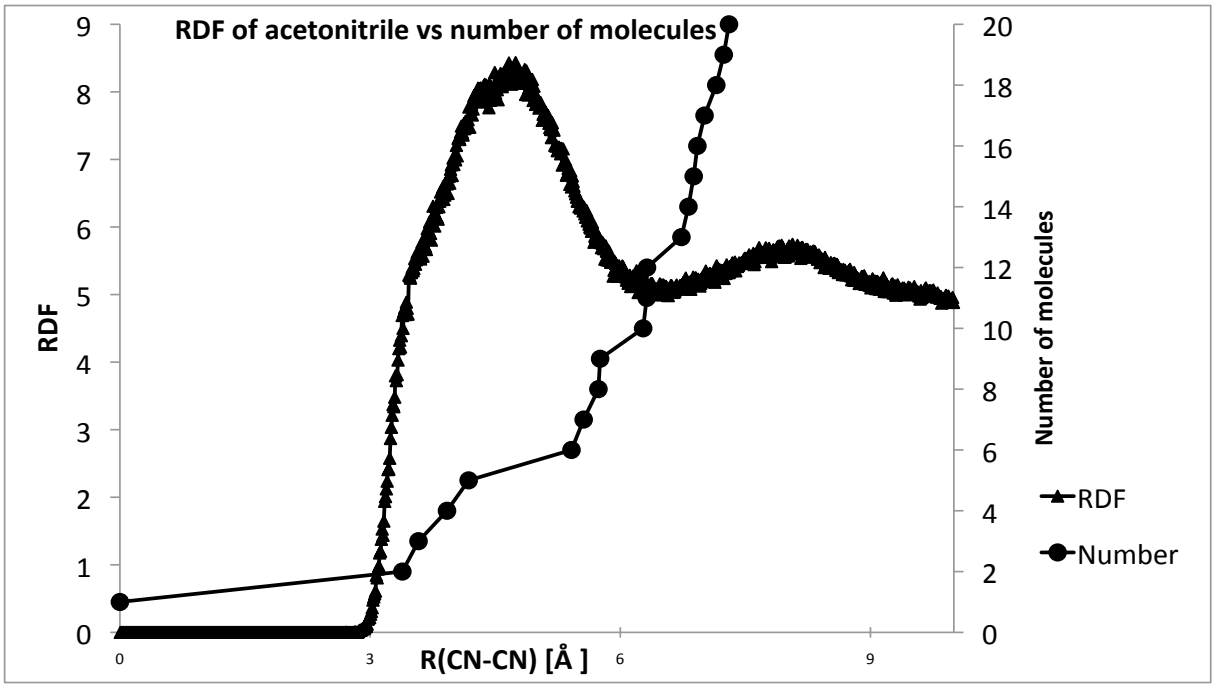

(a) RDF

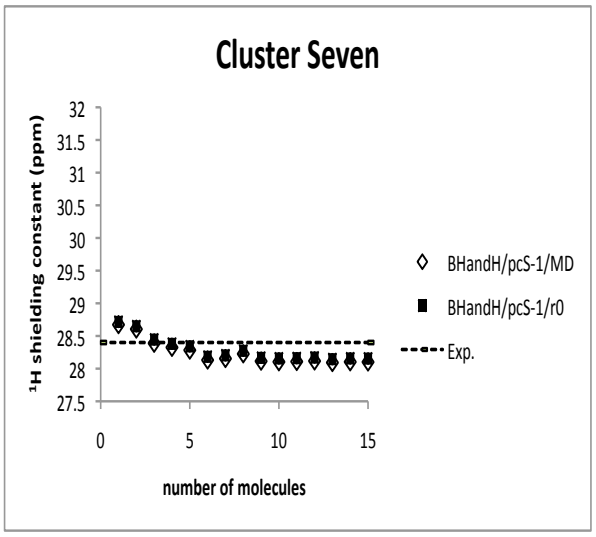

(b) $\sigma(^1\mathrm{H})$

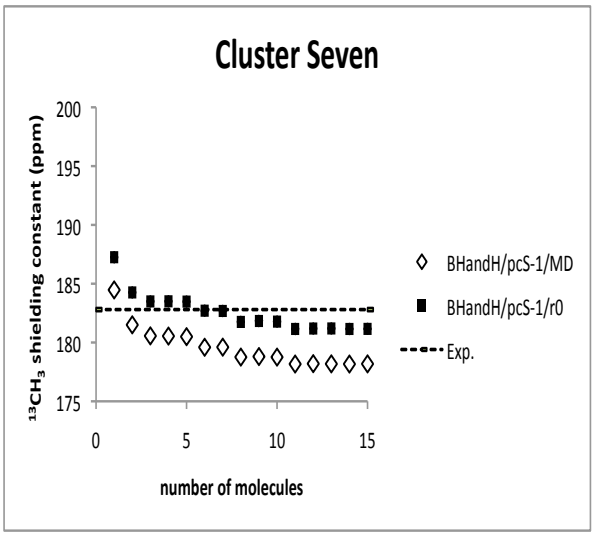

(c) $\sigma(^{13}\mathrm{CH_3})$

Figure 6.9: (a) The radial distribution function (left) of acetonitrile and the number of molecules (right) versus the distance from the central molecule in cluster seven. (b) The change in $\sigma(^1\mathrm{H})$ of the central molecule versus the size of the cluster of acetonitrile at the BHandH/pcS-1 level. (c) The change in $\sigma(^{13}\mathrm{CH_3})$ of the central molecule versus the size of the cluster of acetonitrile at the BHandH/pcS-1 level.

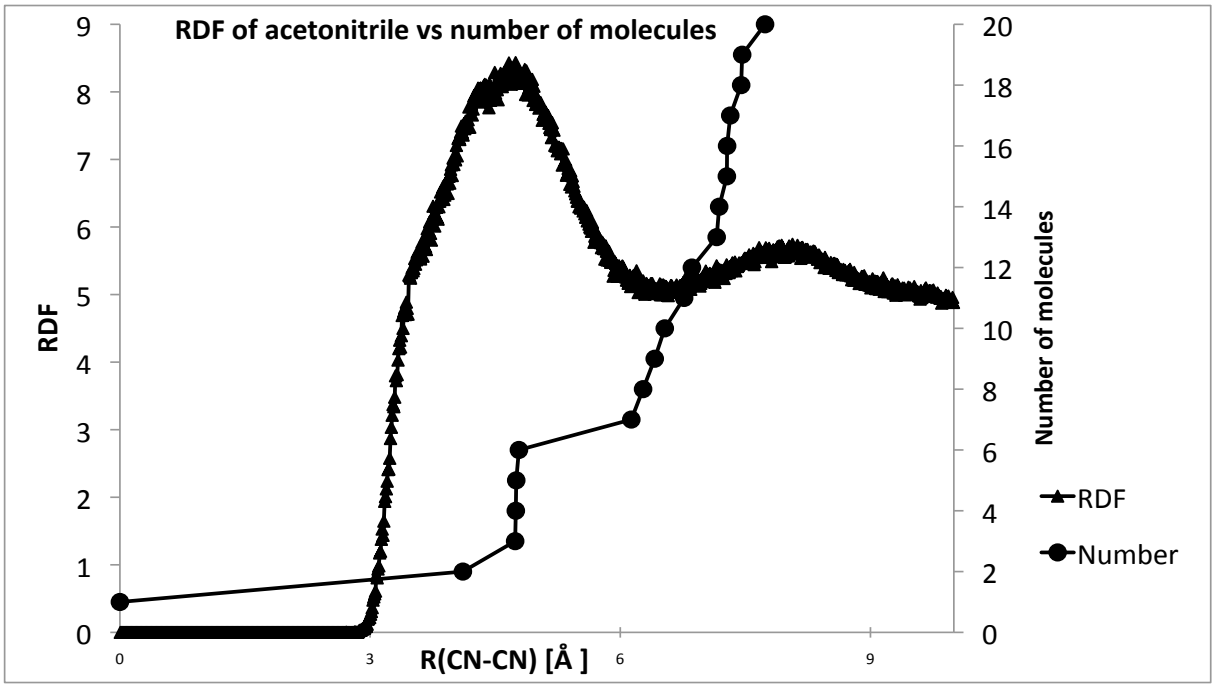

(a) RDF

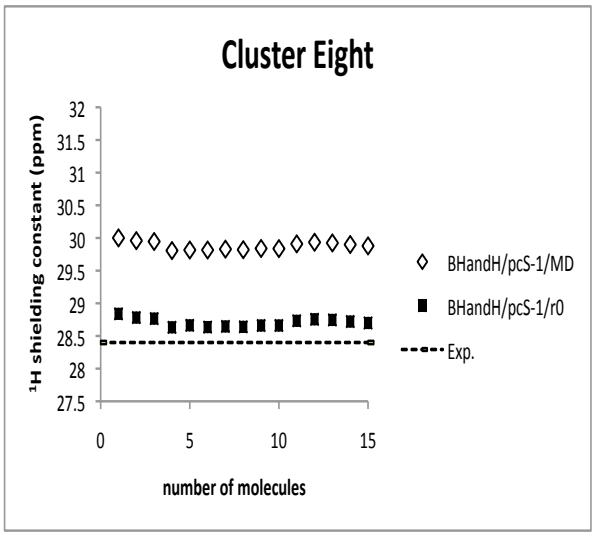

(b) $\sigma(^1\mathrm{H})$

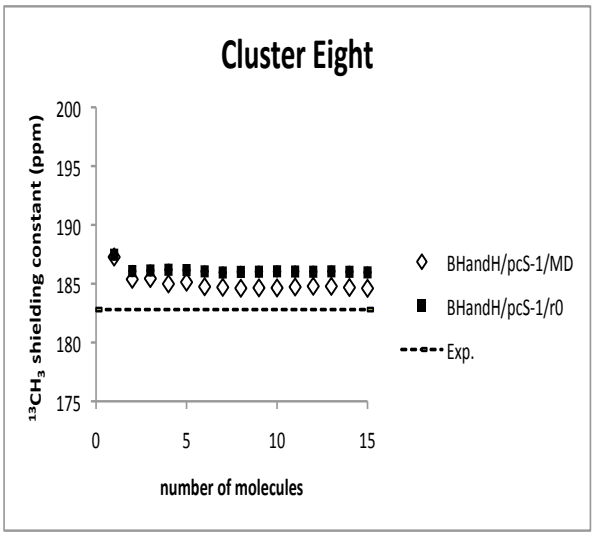

(c) $\sigma(^{13}\mathrm{CH_3})$

Figure 6.10: (a) The radial distribution function (left) of acetonitrile and the number of molecules (right) versus the distance from the central molecule in cluster eight. (b) The change in $\sigma(^1\mathrm{H})$ of the central molecule versus the size of the cluster of acetonitrile at the BHandH/pcS-1 level. (c) The change in $\sigma(^{13}\mathrm{CH_3})$ of the central molecule versus the size of the cluster of acetonitrile at the BHandH/pcS-1 level.

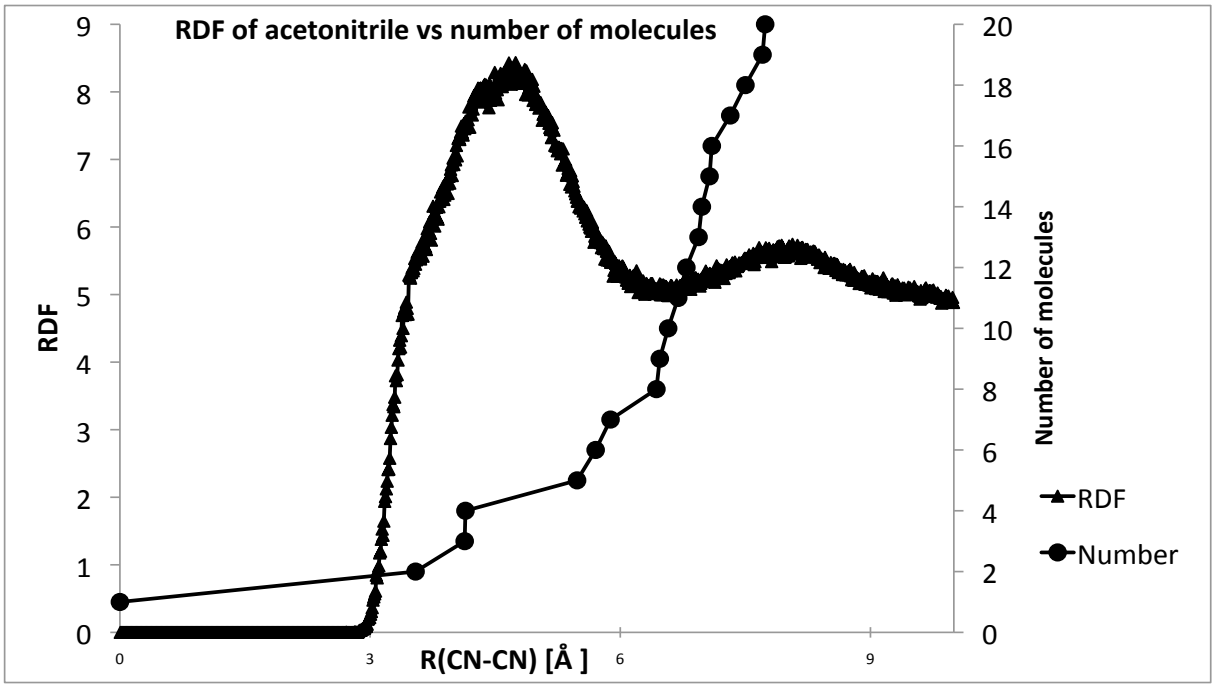

(a) RDF

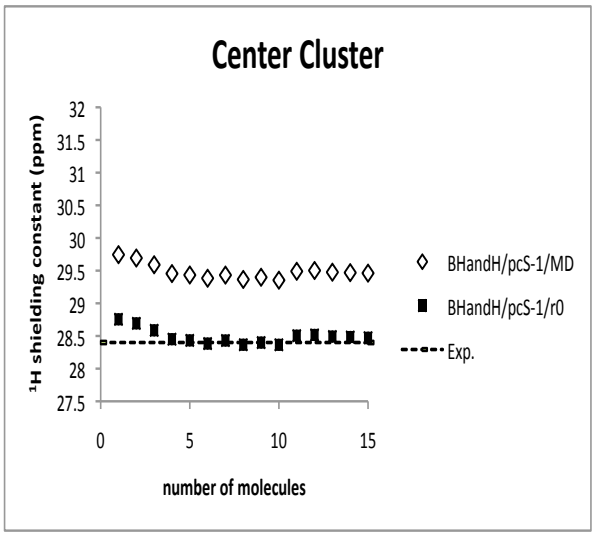

(b) $\sigma(^1\mathrm{H})$

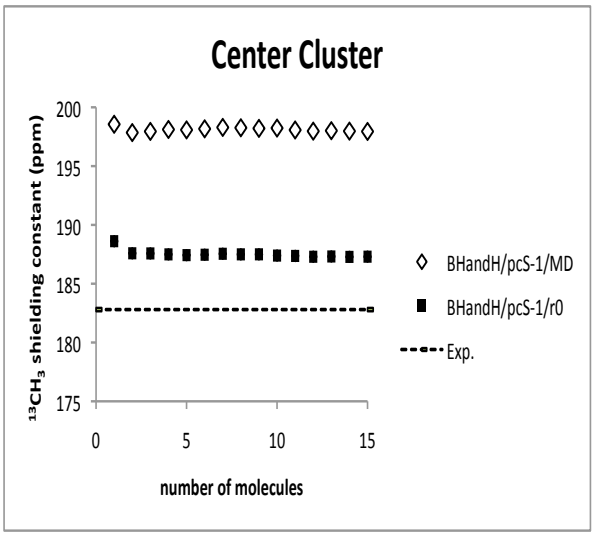

(c) $\sigma(^{13}\mathrm{CH_3})$

Figure 6.11: (a) The radial distribution function (left) of acetonitrile and the number of molecules (right) versus the distance from the central molecule in center cluster . (b) The change in $\sigma(^1\mathrm{H})$ of the central molecule versus the size of the cluster of acetonitrile at the BHandH/pcS-1 level. (c) The change in $\sigma(^{13}\mathrm{CH_3})$ of the central molecule versus the size of the cluster of acetonitrile at the BHandH/pcS-1 level.

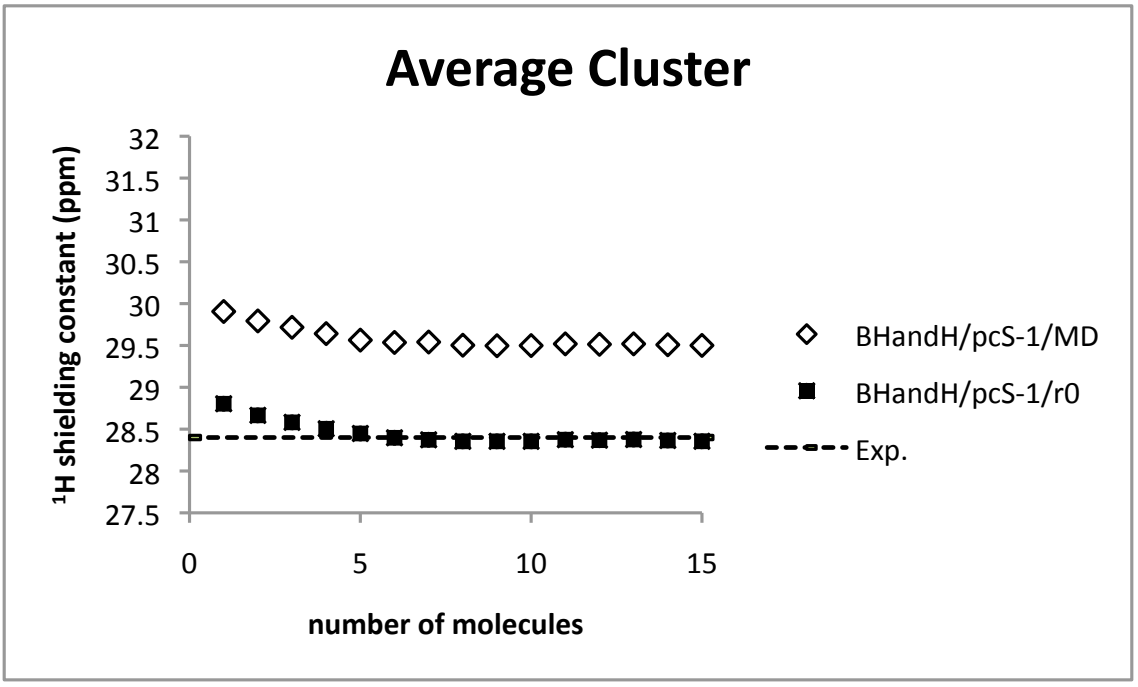

Figure 6.12: The average change in $\sigma(^{1}\mathrm{H})$ in the central molecules of different nine clusters of acetonitrile versus the size of the clusters at the BHandH/pcS-1 level.

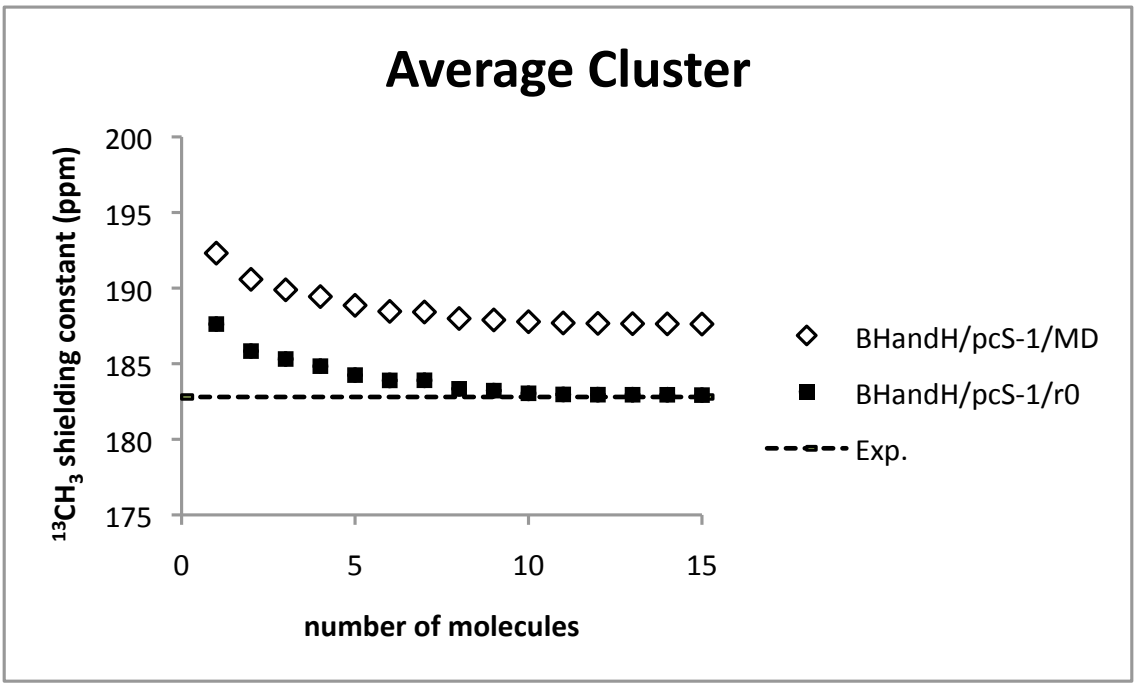

Figure 6.13: The average change in $\sigma(^{13}\mathrm{CH_3})$ in the central molecules of different nine clusters of acetonitrile versus the size of the clusters at the BHandH/pcS-1 level.

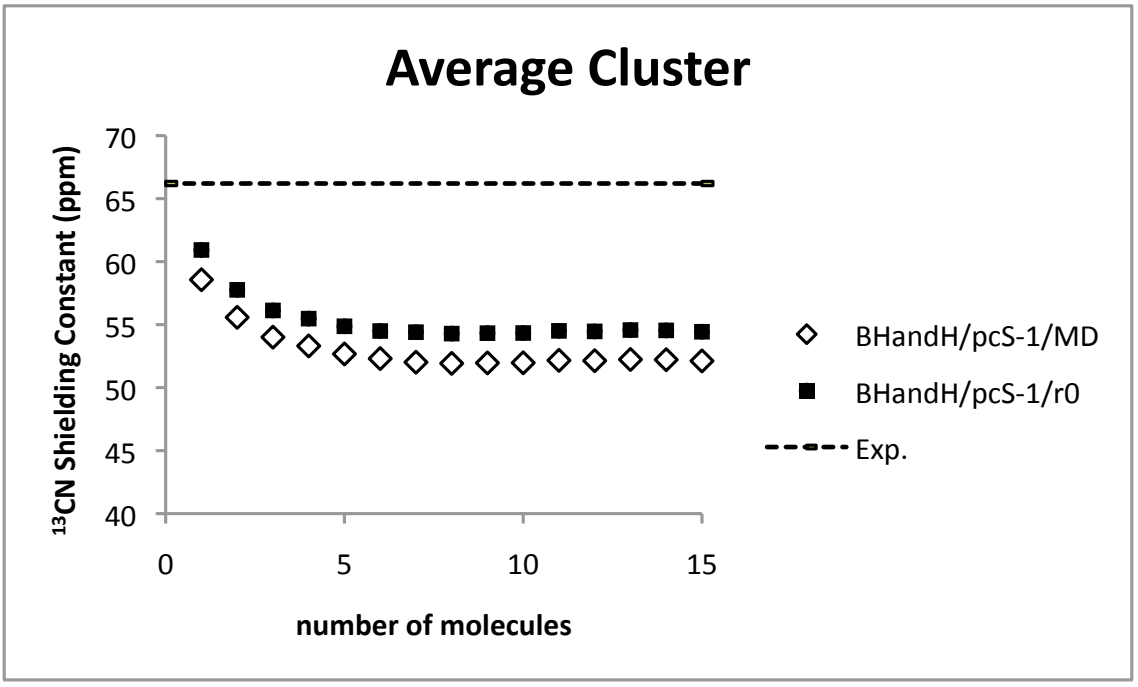

Figure 6.14: The average change in $\sigma(^{13}\mathrm{CN})$ in the central molecules of different nine clusters of acetonitrile versus the size of the clusters at the BHandH/pcS-1 level.

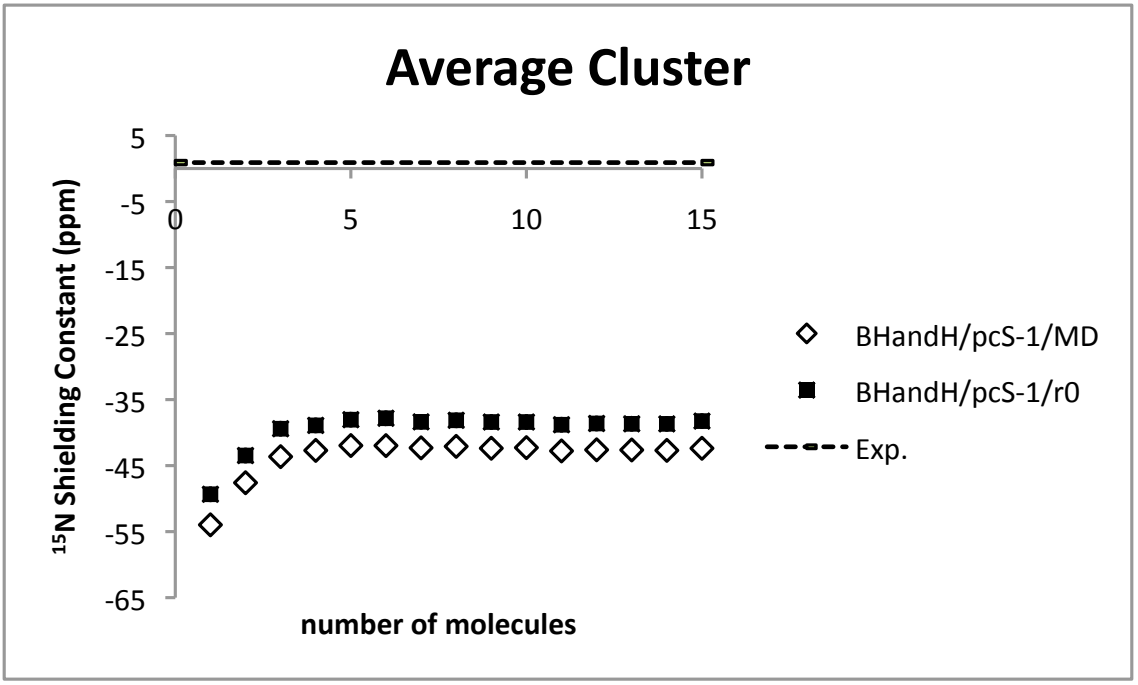

Figure 6.15: The average change in $\sigma(^{15}\mathrm{N})$ in the central molecules of different nine clusters of acetonitrile versus the size of the clusters at the BHandH/pcS-1 level.

Chapter 7

Summary and Conclusions

Although continuum solvation models are widely used and implemented in many software packages and provide results relatively quickly, they are not accurate enough. More accurate results can be obtained by quantum mechanical and molecular dynamics (QM/MD) methods. This strategy is known as explicit solvation model. QM/MD techniques have been applied to study the change in nuclear shielding constants of acetonitrile from the gas phase to liquid phase.

First, the selection of an efficient method/basis was established for acetonitrile in the gas phase. A wide range of basis sets were tested and the pcS-1 basis set was selected to be applied for the calculations on the clusters extracted from molecular dynamics simulations. Different *ab initio* methods (HF, MP2, CCSD, CCSD(T)) as well as two DFT methods (B3LYP and BHandH) were applied and compared to the experimental data of the shielding constants of acetonitrile. From the results, it has been shown that triple bonded nuclei required the treatment at the coupled-cluster level. The BHandH method provided good results for ^{1}H and $^{13}CH_3$ nuclei and was further applied for cluster calculations. However, the development of new DFT methods is an area of continuous research and more efficient

functionals are possible. The remaining error from the experimental values could be attributed to vibrational effects. The motions of nuclei due to molecular vibrations change the shielding constants values and thus corrections are required for accurate results.

Molecules in the liquid phase neither have a well-defined structure like solids nor the complete random motions of gases but a short range structure. To account for the structure of liquids, several different clusters in shape and size have been extracted from MD simulations of acetonitrile. Quantum mechanical methods at the BHandH/pcS-1 level were applied for the selected clusters to calculate the shielding constants of the central molecule. The different distributions of the clusters produced different convergence toward the experimental data. The role of the geometry of the central molecule was tested and has been shown to be an important factor in approaching the experimental values.

Bibliography

[1] Richards, S. A.; Hollerton, J. C. *Essential Practical NMR for Organic Chemistry*; John Wiley & Sons: Chichester, U. K., 2011.

[2] http://nobelprize.org

[3] http://goldbook.iupac.org/C01036.html

[4] Saielli, G.; Nicolaou, K. C.; Ortiz, A.; Zhang, H.; Bagno, A. *J. Am. Chem. Soc.* **2011**, 133, 6072.

[5] Lodewyk, M. W.; Siebert, M. R.; Tantillo, D. J. *Chem. Rev.* **2012**, 112, 1839.

[6] Bast, R.; Ekstrøm, U.; Gao, B.; Helgaker, T.; Ruud, T.; A. J. Thorvaldsen, A. J. *Phys. Chem. Chem. Phys.* **2011**, 13, 2627.

[7] Bühl, M.; van Mourik, T. *WIREs Comput. Mol. Sci.*, **2011**, 1, 634.

[8] Hehre, W. J.; Radom, L.; Schleyer, P. V.; Pople, J. A. *Ab initio Molecular Orbital Theory*; Wiley: New York, NY, 1986.

[9] Cramer, C. J. *Essentials of Computational Chemistry: Theories and Models*, 2nd ed.; Wiley: Chichester, U.K., 2004.

[10] Pople, J. A.; *Angew. Chem. Int. Ed.* **1999**, 38, 1894.

[11] Stephen G. Spanton, S. G.; Whittern, D.; *Magn. Reson. Chem.* **2009**, 47, 1055.

[12] http://www.cambridgesoft.com/software/ChemDraw/

[13] Doucet, J. P.; Panaye, A.; Feuilleaubois, E.; Ladd, P. *J. Chem. Inf. Comput. Sci.* **1993**, 33, 320.

[14] Perez, M.; Peakman, T. M.; Alex, A.; Higginson, P. D.; Mitchell, J. C.; Snowden, M. J.; Morao, I. *J. Org. Chem.* **2006**, 17, 3103.

[15] Ramsey, N. F. *Phys. Rev.* **1950**, 78, 699.

[16] Hameka, H. F. *Advanced Quantum Chemistry*; Addison-Wesley: Reading, MA, 1965.

[17] Cybulski, S. M.; Bishop, D. M. *Chem. Phys. Lett.* **1996**, 250, 471.

[18] Chesnut, D. B.; Rusiloski, B. E.; Moore, K. D.; Egolf, D. A. *J. Comput. Chem.* **1993**, 14, 1364.

[19] Keith, T. A.; Bader, R. F. W.; *Chem. Phys. Lett.* **1992**, 194, 1.

[20] Schindler, M.; Kutzelnigg, W. *J. Chem. Phys.* **1982**, 76, 1919.

[21] Hansen, A. E.; Bouman, T. D. *J. Chem. Phys.* **1985**, 82, 5035.

[22] London, F. *J. Phys. Radium* **1937**, 8, 397.

[23] Ditchfield, R. *J. Chem. Phys.* **1972**, 56, 5688.

[24] Fukui, H.; Miura, K.; Yamazaki, H.; Nosaka, T. *J. Chem. Phys.* **1985**, 82, 1410.

[25] Wolinski, K.; Hinton, J. F.; Pulay, P. *J. Am. Chem. Soc.* **1990**, 112, 8251.

[26] Helgaker, T.; Jørgensen, P. *J. Chem. Phys.* **1991**, 95, 2595.

[27] Jaszunski, M.; Helgaker, T.; Ruud, K.; Jørgensen, P.; Bak, K. L.; Koch, H. *Mol. Phys.* **1995**, 85, 671.

[28] Zhang, Y.; Wu, A,; Xu, X.; Yan, Y. *J. Phys. Chem. A* **2007**, 111, 9431.

[29] Auer, A.; Gauss, J.; Stanton, J. F. *J. Chem. Phys.* **2003**, 118, 10407.

[30] Davidson, E. R.; Feller, D. *Chem. Rev.* **1986**, 86, 681.

[31] Jain, R.; Bally, T.; Rablen, P. R. *J. Org. Chem.* **2009**, 74, 4017.

[32] Giesen, D. J. ; Zumbulyadis, N. *Phys. Chem. Chem. Phys.* **2002**, 4, 5498.

[33] Szabo, A.; Ostlund, N. S. *Modern Quantum Chemistry: Introduction to Advanced Electronic Structure Theory*; Dover: Mineola, NY, 1996.

[34] Smith, C. M.; Amos, R. D.; Handy, N. C. *Mol. Phys.* **1992**, 77, 381.

[35] Jaszuński, M.; Bak, K. L.; Jørgensen, P.; Helgaker, T.; Ruud, K.; Jensen, H. J. A. *Chem. Phys. Lett.* **1993**, 204, 608.

[36] van Wüllen, C.; Fleischer, U.; Kutzelnigg, W. *Mol. Phys.* **1994**, 81, 1373.

[37] Cheeseman, J.; Trucks, G. W.; Keith, T. A.; Frisch, M. J. *J. Chem. Phys.* **1996**, 104, 5497.

[38] Schäfer, A.; Horn, H.; Ahlrichs, R. *J. Chem. Phys.* **1992**, 97, 2571.

[39] Jensen, F. *J. Chem. Theory Comput.* **2008**, 4, 719.

[40] Jensen, F. *J. Chem. Phys.* **2008**, 129, 064111.

[41] Gauss, J. *Chem. Phys. Lett.* **1992**, 191, 614.

[42] Gauss, J. *J. Chem. Phys.* **1993**, 99, 3629.

[43] Fukui, H.; Baba, T.; Matsuda, H.; Miura, K. *J. Chem. Phys.* **1994**, 100, 6608.

[44] Olsen, J.; Jørgensena P.; Helgaker, T.; Christiansen, O. *J. Chem. Phys.* **2000**, 112, 9736.

[45] Ruud, K.; Helgaker, T.; Kobayashi, R.; Jørgensen, P.; Bak, K.; Jensen, H. J. Aa. *J. Chem. Phys.* **1994**, 100, 8178.

[46] Azizi, Z.; Roos, B.; Veryazov, V. *Phys. Chem. Chem. Phys.* **2006**, 8, 2727.

[47] Harding, M. E.; Gauss, J.; Schleyer, P. v. R. *J. Phys. Chem. A* **2011**, 115, 2340.

[48] Bartlett, R. J.; Musia, M. *Rev. Mod. Phys.* **2007**, 79, 291.

[49] Gauss, J.; Stanton, J. F. *J. Chem. Phys.* **1995**, 102, 251.

[50] Gauss, J.; Stanton, J. F. *J. Chem. Phys.* **1995**, 103, 3561.

[51] Gauss, J.; Stanton, J. F. *J. Chem. Phys.* **1996**, 104, 2574.

[52] Gauss, J.; Stanton, J. F. *Phys. Chem. Chem. Phys.* **2000**, 2, 2047.

[53] Gauss, J. *J. Chem. Phys.* **2002**, 116, 4773.

[54] Harding, M. E.; Lenhart, M.; Auer, A. A.; Gauss, J. *J. Chem. Phys.* **2008**, 128, 244111.

[55] Auer, A. A. *J. Chem. Phys.* **2009**, 131, 24116.

[56] de Dios, A. C. *Prog. NMR Spectrosc.* **1996**, 29, 229.

[57] Kupka, T.; Stachow M.; Nieradka, M.; Kaminsky, J.; Pluta, T. *J. Chem. Theory Comput.* **2010**, 6, 1580.

[58] Truhlar, D. G.; Zhao, Y. *J. Phys. Chem. A* **2008**, 112, 6794.

[59] Wu, A.; Zhang, Y.; Xu, X.; Yan, Y. *J. Comput. Chem.* **2007**, 28, 2431.

[60] Sarotti, A. M.; Pellegrinet, S. C. *J. Org. Chem.* **2009**, 74, 7254.

[61] Armangue, L.; Sola, M.; Swart, M. *J. Phys. Chem. A* **2011**, 115, 1250.

[62] Cohen, A. J.; Mori-Snchez, P.; Yang, W. *Chem. Rev.*, **2012**, 112, 289.

[63] Jain, R.; Bally, T.; Rablen, P. R. *J. Org. Chem.* **2009**, 74, 4017.

[64] Kupka, T. *Magn. Reson. Chem.* **2009**, 47, 674.

[65] Kupka, T. *Magn. Reson. Chem.* **2009**, 47, 959.

[66] Ruden, T. A.; Ruud, K. In *Calculation of NMR and EPR Parameters: Theory and Applications*; Kaupp, M., Buhl, M., Malkin, V. G., Eds.; Wiley-VCH: Weinheim, Germany, 2004.

[67] Sundholm, D.; Guass, J.; Schäfer, A. *J. Chem. Phys.* **1996**, 105, 11051.

[68] Faska, N.; Auhmani, A.; Esseffar, M.; Abboud, J. L.-M. *J. Phys. Org. Chem.* **2011**, 24, 1209.

[69] Ribeiro, R. F.; Marenich, A. V.; Cramer, C. J.; Truhlar. D. G. *J. Chem. Theory Comput.* **2009**, 5, 2284.

[70] Bothner-By, A. A.; Glick, R. E. *J. Chem. Phys.* **1957**, 26, 1651

[71] Reeves, L. W.; Schneider, W. G. *Can. J. Chem.* **1957**, 35, 251

[72] Buckingham, A. D.; Schafer, T.; Schneider, W. G. *J. Chem. Phys.* **1960**, 32, 1227.

[73] Tomasi, J.; Mennucci, B.; Cammi, R. *Chem. Rev.* **2005**, 105, 2999.

[74] Mikkelsen, K. V.; Jørgensen, P.; Ruud, K.; Helgaker, T. *J. Chem. Phys.* **1997**, 106, 1170.

[75] Mikkelsen, K. V.; Ruud, K.; Helgaker, T. *Chem. Phys. Lett.* **1996**, 253, 443.

[76] Benzi, C.; Crescenzi, O.; Pavone, M.; Barone, V. *Magn. Reson. Chem.* **2004**, 42, S57.

[77] Mikkelsen, K. V.; Ruud, K.; Helgaker, T. *J. Comput. Chem.* **1999**, 20, 1281.

[78] Zarzycki, P.; Rustad, J. R. *J. Phys. Chem. A* **2009**, 113, 291.

[79] Borowski, P.; Janowski, T.; Wolinski, K. *Mol. Phys.* **2000**, 98, 1331.

[80] Steiner, P. A.; Gordy, W. *J. Mol. Spectrosc.* **1966** 21, 291

[81] Hurle, R. L.; Woolf, L. A. *J. Chem. Soc., Faraday Trans.* **1982**, 178, 2233.

[82] Radnai, T.; Jedlovszky, P. *J. Phys. Chem.* **1994**, 98, 5994.

[83] Buck, U.; Gu, X. J.; Krohne, R.; Lauenstein, Ch. *Chem. Phys. Lett.* **1990**, 174, 247.

[84] Wright, D.; El-Shall, M. S. *J. Chem. Phys.* **1994**, 100, 3791.

[85] Bohm, H. J.; McDonald, I. R.; Madden, P. A. *Mol. Phys.* **1983**, 49, 347.

[86] Jorgensen W. L.; Briggs, J. M. *Mol. Phys.* **1988**, 63, 547.

[87] Ohba, T.; Ikawa, S. *Mol. Phys.* **1991**, 73, 999.

[88] Siebers, J. G.; Buck, U.; Beu, T. A. *Chem. Phys.* **1998**, 239, 549.

[89] Mata, R. A.; Costa Cabral, B. J. *J. Mol. Struct. (THEOCHEM)* **2004**, 673, 155.

[90] Takayanagi, T. *J. Chem. Phys.* **2005**, 122, 244307.

[91] **a)** Gaussian 03, Revision C.02, M. J. Frisch, G. W. Trucks, H. B. Schlegel, G. E. Scuseria, M. A. Robb, J. R. Cheeseman, J. A. Montgomery, Jr., T. Vreven, K. N. Kudin, J. C. Burant, J. M. Millam, S. S. Iyengar, J. Tomasi, V. Barone, B. Mennucci, M. Cossi, G. Scalmani, N. Rega, G. A. Petersson, H. Nakatsuji, M. Hada, M. Ehara, K. Toyota, R. Fukuda, J. Hasegawa, M. Ishida, T. Nakajima, Y. Honda, O. Kitao, H. Nakai, M. Klene, X. Li, J. E. Knox, H. P. Hratchian, J. B. Cross, V. Bakken, C. Adamo, J. Jaramillo, R. Gomperts, R. E. Stratmann, O. Yazyev, A. J. Austin, R. Cammi, C. Pomelli, J. W. Ochterski, P. Y. Ayala, K. Morokuma, G. A. Voth, P. Salvador, J. J. Dannenberg, V. G. Zakrzewski, S. Dapprich, A. D. Daniels, M. C. Strain, O. Farkas, D. K. Malick, A. D. Rabuck, K. Raghavachari, J. B. Foresman, J. V. Ortiz, Q. Cui, A. G. Baboul, S. Clifford, J. Cioslowski, B. B. Stefanov, G. Liu, A. Liashenko, P. Piskorz, I. Komaromi, R. L. Martin, D. J. Fox, T. Keith, M. A. Al-Laham, C. Y. Peng, A. Nanayakkara, M. Challacombe, P. M. W. Gill, B. Johnson, W. Chen, M. W. Wong, C. Gonzalez, and J. A. Pople, Gaussian, Inc., Wallingford CT, 2004. **b)** Gaussian 09, Revision A.02, Frisch, M. J.; Trucks, G. W.; Schlegel, H. B.; Scuseria, G. E.; Robb, M. A.; Cheeseman, J. R.; Scalmani, G.; Barone, V.; Mennucci, B.; Petersson, G. A.; Nakatsuji, H.; Caricato, M.; Li, X.; Hratchian, H. P.; Izmaylov, A. F.; Bloino, J.; Zheng, G.; Sonnenberg, J. L.; Hada, M.; Ehara, M.; Toyota, K.; Fukuda, R.; Hasegawa, J.; Ishida, M.; Nakajima, T.; Honda, Y.; Kitao, O.; Nakai, H.; Vreven, T.; Montgomery, Jr., J. A.; Peralta, J. E.; Ogliaro, F.; Bearpark, M.; Heyd, J. J.; Brothers, E.; Kudin, K. N.; Staroverov, V. N.; Kobayashi, R.; Normand, J.; Raghavachari, K.; Rendell, A.; Burant, J. C.; Iyengar, S. S.; Tomasi, J.; Cossi, M.; Rega, N.; Millam, N. J.; Klene, M.; Knox, J. E.; Cross, J. B.; Bakken, V.; Adamo, C.; Jaramillo, J.; Gomperts, R.; Stratmann, R. E.; Yazyev, O.; Austin, A. J.; Cammi, R.; Pomelli, C.; Ochterski, J. W.; Martin, R. L.; Morokuma, K.; Zakrzewski, V. G.; Voth, G. A.; Salvador, P.; Dannenberg, J. J.; Dapprich, S.; Daniels, A. D.; Farkas, .; Foresman, J. B.; Ortiz, J. V.; Cioslowski, J.; Fox, D. J. Gaussian, Inc., Wallingford CT, 2009.

[92] CFOUR, a quantum chemical program package written by J.F. Stanton, J. Gauss, M.E. Harding, P.G. Szalay with contributions from A.A. Auer, R.J. Bartlett, U. Benedikt, C. Berger, D.E. Bernholdt, Y.J. Bomble, O. Christiansen, M. Heckert, O. Heun, C. Huber, T.-C. Jagau, D. Jonsson, J. Juslius, K. Klein, W.J. Lauderdale, D.A. Matthews, T. Metzroth, D.P. O'Neill, D.R. Price, E. Prochnow, K. Ruud, F. Schiffmann, S. Stopkowicz, J. Vzquez, F. Wang, J.D. Watts and the integral packages MOLECULE (J. Almlf and P.R. Taylor), PROPS (P.R. Taylor), ABACUS (T. Helgaker, H.J. Aa. Jensen, P. Jrgensen, and J. Olsen), and ECP routines by A. V. Mitin and C. van Wllen.

[93] Costain, C. C. *J. Chem. Phys.* **1958**, 29, 864.

[94] Dunning Jr., T. H. *J. Chem. Phys.* **1989**, 90, 1007.

[95] Dunning Jr., T. H. *J. Chem. Phys.* **1992**, 96, 6796.

[96] Dunning Jr., T. H. *J. Chem. Phys.* **1995**, 103, 4572.

[97] Ahlrichs, R. *J. Chem. Phys.* **1994**, 100, 5829.

[98] Ahlrichs. R. *Phys. Chem. Chem. Phys.* **2005**, 7, 3297.

[99] Jackowski, K. *Appl. Magn. Reson.* **2003**, 24, 379.

[100] Ruud, K.; Åstrand, P.-O.; Taylor, P. R. *J. Chem. Phys.* **2000**, 112, 2668.

[101] DALTON, a molecular electronic structure program, Release 2.0 (2005), see http://daltonprogram.org/

[102] Prochnow, E.; Auer, A. A. *J. Chem. Phys.* **2010**, 132, 64109.

[103] Kupka, T.; Ruscic, B.; Botto, R. E. *J. Phys. Chem. A* **2002**, 106, 10396.

[104] Ruud, K.; Åstrand, P.-O.; Taylor, P. R. *J. Am. Chem. Soc.* **2001**, 123, 4826.

[105] Gregušová, A.; Perera, S. A.; Bartlett, R. J. *J. Chem. Theory Comput.* **2010**, 6, 1228.

[106] Becke, A. D. *J. Chem. Phys.* **1993**, 98, 5648.

[107] Helgaker, T.; Coriani, S.; Jørgensen, P.; Kristensen, K.; Olsen, J.; Ruud, K. *Chem. Rev.* **2012**, 112, 543.

[108] Kern, W. C.; Matcha, R. L. *J. Chem. Phys.* **1969**, 49, 2081.

[109] Silverstein. R. M.; Webster, F. X.; Kiemle, D. *Spectrometric Identification of Organic Compounds*, 7th ed.; Wiley: New York, 2005.

[110] Bak, K. L.; Gauss, J.; Jørgensen, P.; Olsen, J.; Helgaker, T.; Stanton, J. F. *J. Chem. Phys.* **2001**, 114, 6548.

[111] *Accurate Molecular Structures: Their Determination and Importance*; Domenicano, A.; Hargittai, I., Eds.; Oxford University Press: Oxford, U. K., 1992.

[112] Demaison, J.; Dubrulle, A.; Boucher, D.; Burie, J.; Typke, V. *J. Mol. Spectrosc.* **1979**, 15, 1.

[113] Guennec, M. Le; Wlodarczak, G.; Burie, J.; Demaison, J. *J. Mol. Spectrosc.* **1992**, 154, 305.

[114] Karakida, K.; Fukuyama, T.; Kuchitsu, K. *Bull. Chem. Soc. Jpn.* **1974**, 47, 299.

[115] Lounila, J.; Ala-Korpela, M.; Jokisaari, J. *J. Chem. Phys.* **1990**, 93, 8514.

[116] Margulés, L.; Demaison, J.; Boggs, J. E. *Struct. Chem.* **2000**, 11, 145.

[117] Puzzarini, C.; Cazzoli, G. *J. Mol. Spectrosc.* **2006**, 240, 260.

[118] Allen, M. P.; Tildesley, D. J. *Computer Simulation of Liquids*; Clarendon Press: Oxford, U. K., 1987.

[119] Cui, Q.; Karplus, M. *J. Phys. Chem. B* **2000**, 104, 3721.

[120] Pfrommer, B. G.; Mauri, F.; Louie S. G. *J. Am. Chem. Soc.* **2000**, 122, 123.

[121] TINKER - Software Tools for Molecular Design, v. 4.2; http://dasher.wustl.edu/tinker/

[122] Schaftenaar, G. MOLDEN 4.8, CAOSCAMM Center, The Netherlands, 1998.

[123] Jorgensen, W. L.; Maxwell, D. S.; TiradoRives, J. *J. Am. Chem. Soc.* **1996**, 118, 11225.

[124] John G. Kirkwood, J. G.; Boggs, E. M. *J. Chem. Phys.* **1942**, 10, 394.